



UPPSALA
UNIVERSITET

*Digital Comprehensive Summaries of Uppsala Dissertations
from the Faculty of Science and Technology 1501*

From Light to Dark

Electrical Phenomena in Cu(In,Ga)Se₂ Solar Cells

PIOTR SZANIAWSKI



ACTA
UNIVERSITATIS
UPSALIENSIS
UPPSALA
2017

ISSN 1651-6214
ISBN 978-91-554-9884-9
urn:nbn:se:uu:diva-319454

Dissertation presented at Uppsala University to be publicly examined in Högssalen, 10132, Ångströmlaboratoriet, Lägerhyddsvägen 1, Uppsala, Thursday, 1 June 2017 at 13:15 for the degree of Doctor of Philosophy. The examination will be conducted in English. Faculty examiner: Professor Thomas Walter (Ulm University).

Abstract

Szaniawski, P. 2017. From Light to Dark. Electrical Phenomena in Cu(In,Ga)Se₂ Solar Cells. *Digital Comprehensive Summaries of Uppsala Dissertations from the Faculty of Science and Technology* 1501. 83 pp. Uppsala: Acta Universitatis Upsaliensis. ISBN 978-91-554-9884-9.

In Cu(In,Ga)Se₂ (CIGS) solar cells the CIGS layer serves as the light absorber, growing naturally *p*-type. Together with an *n*-type buffer layer they form a *p-n* heterojunction. Typically, CdS is used as a buffer, although other, less toxic materials are investigated as alternatives. The intrinsic *p*-type doping of CIGS layers is the result of complex defect physics. Defect formation energies in CIGS are very low or even negative, which results in extremely high defect concentrations. This leads to many unusual electrical phenomena that can be observed in CIGS devices. This thesis mostly focuses on three of these phenomena: light-soaking, light-on-bias, and light-enhanced reverse breakdown.

Light-soaking is a treatment that involves illuminating the investigated device for an extended period of time. In most CIGS solar cells it results in an improvement of open-circuit voltage, fill factor, and efficiency that can persist for hours, if not days. The interplay between light-soaking and the remaining two phenomena was studied. It was found that light-soaking has a strong effect on light-on-bias behavior, while the results for light-enhanced breakdown were inconclusive, suggesting little to no impact.

Light-on-bias is a treatment which combines simultaneous illumination and application of reverse bias to the studied sample. Illuminating CdS-based samples with red light while applying a reverse bias results in a significant increase in capacitance due to filling of traps. In many cases, this is accompanied by a decrease in device performance under red illumination. Complete recovery is possible by illuminating the treated sample with blue light, which causes hole injection from the CdS buffer. In samples with alternative buffer layers, there is little distinction between red and blue illumination, and the increase in capacitance is milder. At the same time, there is little effect on device performance.

Reverse breakdown can occur when a sufficiently large reverse bias is applied to a *p-n* junction, causing a large reverse current to flow through the device. In CIGS solar cells, the voltage at which breakdown occurs in darkness decreases in the presence of blue illumination. A model explaining the breakdown in darkness was proposed as a part of this thesis. The model assumes that all voltage drops on the buffer layer in darkness and on the CIGS layer under blue illumination. The high electric field in the buffer facilitates Poole-Frenkel conduction and Fowler-Nordheim tunneling between the absorber and the buffer.

Keywords: Solar cells, Photovoltaics, Cu(InGa)Se₂, CIGS, Electrical characterization

Piotr Szaniawski, Department of Engineering Sciences, Solid State Electronics, Box 534, Uppsala University, SE-75121 Uppsala, Sweden.

© Piotr Szaniawski 2017

ISSN 1651-6214

ISBN 978-91-554-9884-9

urn:nbn:se:uu:diva-319454 (<http://urn.kb.se/resolve?urn=urn:nbn:se:uu:diva-319454>)

Something witty and meta here

List of Papers

This thesis is based on the following papers, which are referred to in the text by their Roman numerals.

- I **Light-Enhanced Reverse Breakdown in Cu(In,Ga)Se₂ Solar Cells**
P. Szaniawski, J. Lindahl, T. Törndahl, U. Zimmermann, and M. Edoff
Thin Solid Films, vol. 535, pp. 326–330, May 2013
- II **Influence of Varying Cu Content on Growth and Performance of Ga-Graded Cu(In,Ga)Se₂ Solar Cells**
P. Szaniawski, P. Salome, V. Fjallstrom, T. Törndahl, U. Zimmermann, and M. Edoff
IEEE J. Photovolt., vol. 5, no. 6, pp. 1775–1782, Nov. 2015
- III **A Systematic Study of Light-On-Bias Behavior in Cu(In,Ga)Se₂ Solar Cells With Varying Absorber Compositions**
P. Szaniawski, J. Olsson, C. Frisk, V. Fjällström, D. Ledinek, F. Larsson, U. Zimmermann, and M. Edoff
IEEE J. Photovolt., vol. PP, no. 99, pp. 1–10, 2017
- IV **Advancing the Understanding of Reverse Breakdown in Cu(In,Ga)Se₂ Solar Cells**
P. Szaniawski, P. Zabierowski, J. Olsson, U. Zimmermann, and M. Edoff
IEEE J. Photovolt., accepted, 2017

Reprints were made with permission from the respective publishers.

Related Papers

The following papers were published during my studies, but are not included as part of this thesis.

Inline Cu(In,Ga)Se₂ Co-evaporation for High-Efficiency Solar Cells and Modules

J. Lindahl, U. Zimmermann, P. Szaniawski, T. Törndahl, A. Hultqvist, P. Salome, C. Platzer-Björkman, and M. Edoff
IEEE J. Photovolt., vol. 3, no. 3, pp. 1100–1105, Jul. 2013

The effect of Mo back contact ageing on Cu(In,Ga)Se₂ thin-film solar cells

P. Salome, V. Fjallstrom, A. Hultqvist, P. Szaniawski, U. Zimmermann, and M. Edoff
Prog. Photovolt., vol. 22, no. 1, pp. 83–89, Jan. 2014

Zn(O, S) Buffer Layers and Thickness Variations of CdS Buffer for Cu₂ZnSnS₄ Solar Cells

T. Ericson, J. Scragg, A. Hultqvist, J. T. Wätjen, P. Szaniawski, T. Törndahl, and C. Platzer-Björkman
IEEE J. Photovolt., vol. 4, no. 1, pp. 465–469, Jan. 2014

Optimizing Ga-profiles for highly efficient Cu(In,Ga)Se₂ thin film solar cells in simple and complex defect models

C. Frisk, C. Platzer-Björkman, J. Olsson, P. Szaniawski, J. T. Wätjen, V. Fjällström, P. Salome, and M. Edoff
J. Phys. -Appl. Phys., vol. 47, no. 48, p. UNSP 485104, Dec. 2014

Recovery After Potential-Induced Degradation of CuIn_{1-x}Ga_xSe₂ Solar Cells With CdS and Zn(O,S) Buffer Layers

V. Fjällström, P. Szaniawski, B. Vermang, P. Salome, F. Rostvall, U. Zimmermann, and M. Edoff
IEEE J. Photovolt., vol. 5, no. 2, pp. 664–669, Mar. 2015

A comparison between thin film solar cells made from co-evaporated $\text{CuIn}_{1-x}\text{Ga}_x\text{Se}_2$ using a one-stage process versus a three-stage process

P. Salome, V. Fjällström, P. Szaniawski, J. Leitao, A. Hultqvist, P. Fernandes, J. Teixeira, B. Falcao, U. Zimmermann, A. da Cunha, and M. Edoff
Prog. Photovolt., vol. 23, no. 4, pp. 470–478, Apr. 2015

Deposition temperature induced conduction band changes in zinc tin oxide buffer layers for Cu(In,Ga)Se_2 solar cells

J. Lindahl, J. Keller, O. Donzel-Gargand, P. Szaniawski, M. Edoff, and T. Torndahl
Sol. Energy Mater. Sol. Cells, vol. 144, pp. 684–690, Jan. 2016

Combining strong interface recombination with bandgap narrowing and short diffusion length in $\text{Cu}_2\text{ZnSnS}_4$ device modeling

C. Frisk, T. Ericson, S.-Y. Li, P. Szaniawski, J. Olsson, and C. Platzer-Björkman
Sol. Energy Mater. Sol. Cells, vol. 144, pp. 364–370, Jan. 2016

Defect levels in Cu(In,Ga)Se_2 studied using capacitance and photocurrent techniques

A. Urbaniak, K. Macielak, M. Igalson, P. Szaniawski, and M. Edoff
J. Phys.-Condens. Matter, vol. 28, no. 21, p. 215801, Jun. 2016

Contents

1.	Introduction	13
2.	Semiconductor and Solar Cell Physics	14
2.1	Semiconductors	14
2.1.1	Crystal structure	14
2.1.2	Band gap	16
2.1.3	Free carriers	18
2.1.4	Carrier Transport – Drift and Diffusion	19
2.1.5	Recombination	20
2.1.6	Doping	20
2.1.7	Fermi Level	21
2.2	<i>p-n</i> Junctions	22
2.2.1	Depleted Layer and Built-In Potential	23
2.2.2	Current-Voltage Characteristics	24
2.2.3	Homo- and Heterojunctions	25
2.2.4	Junction Breakdown	26
2.3	Solar Cells	27
2.3.1	Solar Radiation Spectrum	27
2.3.2	Absorption of Light	28
2.3.3	The Photovoltaic Effect and Photocurrent Generation	28
2.3.4	Current-Voltage Characteristics and Efficiency	29
2.3.5	Power Losses	30
2.3.6	The One-Diode Model	33
3.	Cu(In,Ga)Se ₂ – Device Structure	35
3.1	Substrate – Soda-Lime Glass	35
3.2	Back Contact – Mo	36
3.3	Absorber Layer – CIGS	36
3.3.1	Band-gap Grading	36
3.4	Buffer Layers – CdS and Cd-free Buffers	37
3.4.1	CdS	37
3.4.2	Zn(O,S) and Zn _x Sn _{1-x} O _y	38
3.5	Front Contact – i-ZnO and ZnO:Al	38

4.	Electrical Characterization of CIGS Solar Cells.....	39
4.1	The ICVT Setup	39
4.2	Current-Voltage (IV).....	41
4.3	Temperature-Dependent Current-Voltage (IVT)	44
4.4	Capacitance-Voltage (CV).....	45
4.5	Quantum Efficiency (QE)	50
4.6	Measurement conditions and reproducibility.....	51
5.	Defect- and Light-Related Phenomena in CIGS Solar Cells	54
5.1	Light-Soaking.....	54
5.2	Light-on-Bias	56
5.3	Light-Enhanced Reverse Breakdown.....	59
6.	Overview of Papers.....	63
6.1	Paper I: Light-Enhanced Reverse Breakdown in Cu(In,Ga)Se ₂ Solar Cells	63
6.2	Paper II: Influence of Varying Cu Content on Growth and Performance of Ga-Graded Cu(In,Ga)Se ₂ Solar Cells	64
6.3	Paper III: A Systematic Study of Light-On-Bias Behavior in Cu(In,Ga)Se ₂ Solar Cells With Varying Absorber Compositions.....	64
6.4	Paper IV: Advancing the Understanding of Reverse Breakdown in Cu(In,Ga)Se ₂ Solar Cells.....	65
7.	Concluding Remarks	66
	Summary in Swedish	69
	Acknowledgements.....	73
	Bibliography	77

Abbreviations

PV	Photovoltaics
CIGS	Cu(In,Ga)Se_2
IV	Current (density)-voltage
IVT	Temperature-dependent current (density)-voltage
CV	Capacitance-voltage
QE	Quantum efficiency
ZTO	$\text{Zn}_x\text{Sn}_{1-x}\text{O}_y$
REL	Relaxed state
LS	Light-soaking
WLS	White-light-soaking
ROB	Red-on-bias
F-N	Fowler-Nordheim (tunneling)
P-F	Poole-Frenkel (conduction)

1. Introduction

The great balls of fire, otherwise known as stars, are certainly among the most awe-inspiring objects in the universe. The violence of fusion reactions that sustain our very own sun, from its brutally hot 15-million °C core to its cool 6000 °C surface, dwarfs anything accomplished by mankind. Even 150 million kilometers away from the sun, on planet Earth, the light and the warmth that reach us can be unbearable in some parts of the world. It should be no surprise then, that solar energy is the largest energy source available to humanity.

Becquerel's discovery of the photovoltaic effect in 1839 made generation of electricity from sunlight into an actual possibility, but it took more than 100 years for the first practical solar cell to be demonstrated by Bell Laboratories in 1954. For the next two decades, these predecessors of modern cells were mostly employed in space applications, until dropping production costs finally sparked increased interest in terrestrial use.

Today, electricity generation from photovoltaics (PV) is a continuously growing market [1], with China, Japan, and USA sharing two-thirds of the total installed PV capacity in 2015. In the same year, PV had a 29% share in the renewable energy market, and a 1.2% share in covering the global energy demand. The PV market is dominated by wafer-based silicon solar cells, which in 2015 constituted more than 90% of produced PV capacity. Thin-film solar cells trail far behind, corresponding to only 6% of total production.

Despite the low market share, thin-film PV has several advantages over crystalline silicon, which mainly owes its popularity to solid performance combined with low cost. Many of the thin-film materials are better suited to solar cell applications than silicon, offering better optical and electronic properties. Lesser amounts of raw materials are needed, the deposition methods are more flexible, and deposition on flexible *substrates* is possible.

One of the most popular thin-film PV materials is Cu(In,Ga)Se₂, often abbreviated as CIGS. Record efficiency of lab-scale CIGS solar cells has reached the level of 22.6% [2], less than three percentage points below the record for monocrystalline silicon¹ [3]. Therefore, electrical characterization of CIGS devices and some of the peculiar electrical phenomena that can be observed in them are the subject of this thesis.

¹ To be fair, the record for CIGS is on a considerably smaller cell than the one for silicon.

2. Semiconductor and Solar Cell Physics

In this chapter, I present the theoretical concepts necessary to understand the following chapters of the thesis. Semiconductor, p - n junction, and solar cell physics form a foundation which is required for the comprehension of not only solar cells in themselves, but also the measurement techniques used to characterize them.

2.1 Semiconductors

Metals, semiconductors, and insulators form the holy trinity of materials that enable modern electronics. Neither group of materials is more important than the others, since all have multiple applications in contemporary technology. And yet, one could argue that semiconductors are more interesting than either metals or insulators. Where metals are usually excellent at conducting current and insulators at confining it, semiconductors can be made to conduct current in some circumstances and to block it in others. This amazing property and the reasons for its existence have far-reaching consequences. From transistors, billions of which can be found in a single modern computer processor, through various kinds of sensors, to solar cells and light-emitting diodes, semiconductor devices are responsible for most technological wonders of the 20th and 21st centuries.

2.1.1 Crystal structure

To better understand how semiconductors work and how their properties are studied, it helps to familiarize oneself with the concept of crystalline materials. Crystals have been treasured by mankind for thousands of years, but it was only in the beginning of the 20th century that scientists finally had the tools to investigate their structure at the atomic level. In the years 1912-1913, Max von Laue, William Lawrence Bragg and William Henry Bragg discovered that crystals illuminated with X-rays produced distinctive regular patterns on photographic films. Their conclusion was that atoms were organized in a consistent manner throughout the whole volume of a crystal.

This long-distance ordering of atoms, called the crystal lattice, is what gives many metals, insulators, and semiconductors their unique properties. A key feature of the crystal lattice is periodicity, i.e. the whole lattice can be

described by the simplest possible arrangement of atoms, characteristic for a given material, which repeats itself throughout the entire crystal. Examples of such groups of atoms, called unit cells, are shown in *Figure 2.1* for different materials.

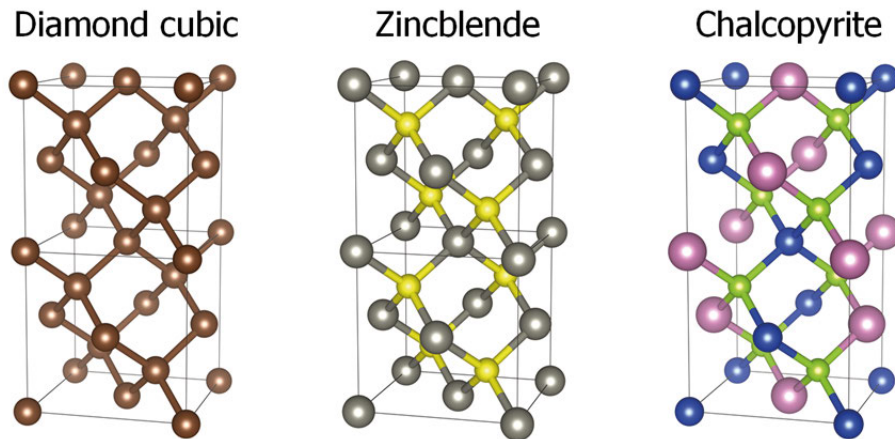


Figure 2.1. Crystal structures of materials sharing the same overall atom arrangement, but based on different numbers of elemental species.

The periodicity of the crystal lattice has a very important consequence: it allows many material properties to be calculated based on the knowledge of the unit cell. While calculations of higher complexity can often be done on matrices of less than 100 atoms, simulating even these relatively small systems demands enormous computational power. With around 10^{22} atoms per cubic centimeter of a solid, simulations of such large volumes are still in the realm of the unthinkable.

Silicon and Two-Element Compound Semiconductors

Silicon crystallizes in the diamond cubic structure, which can be thought of as two intersected face-centered cubic (FCC) lattices (see *Figure 2.1*). Every atom is surrounded by four equidistant neighbors, which together form the corners of a tetrahedron. A step up in complexity is the zincblende structure, also illustrated in *Figure 2.1*, which is shared by many compound semiconductors composed of two elemental species. Each of the two intersected FCC lattices is based on one type of atom.

CIGS

CIGS crystallizes in the chalcopyrite structure, shown in *Figure 2.1*, which is related to the zincblende structure. Since CIGS features up to four different atomic species, however, the complexity is further increased. There are three types of lattice sites, corresponding to atoms of groups I (Cu), III (In and Ga), and VI (Se). Half of the sites that belong to one of the intersected

FCC lattices is occupied by copper atoms, while the other half by either indium or gallium atoms. The unit cell is represented by two zincblende structures stacked on top of each other, with one of them containing more group I sites, and the other more group III sites. In and Ga are interchangeable and distributed randomly among their sites. The complexity of this structure results in many point defects with interesting properties, which will be further discussed later in the thesis.

2.1.2 Band gap

The defining semiconductor property which results from the periodicity of the crystal lattice is the band gap, E_g . It is the single most important concept of semiconductor physics, so it warrants a closer examination. First, consider the atom of the most popular semiconductor material, silicon. The atomic number of silicon is 14, which means it has that many electrons located² around the nucleus. The electrons can be found in electron shells, further subdivided into electron orbitals, which represent the available discrete energy states. The allowed states are strictly governed by the Pauli exclusion principle, and no state can be occupied by more than two electrons of opposite spins. Ten of the electrons fill the two inner electron shells, while the remaining four, known as valence electrons, partly occupy the outermost shell.

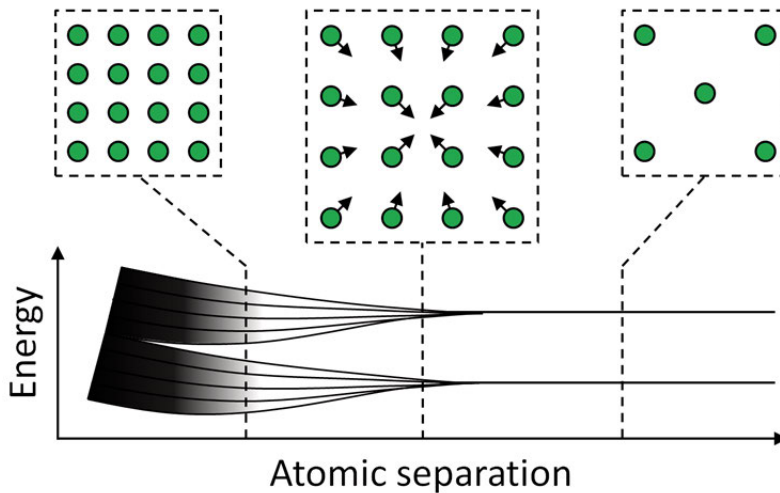


Figure 2.2. When the distance between atoms is sufficiently large, no interaction occurs and electrons occupy discrete energy levels. As the atomic separation decreases and atomic orbitals start to overlap, energy levels split into energy bands.

² In truth, electrons are not well-localized particles. Each electron is described by a wave function, which defines the probability of finding the electron at different locations within a certain volume of space.

Let us now consider a thought experiment that involves multiple silicon atoms, as illustrated in *Figure 2.2*. When the distance between the atoms is several nanometers or more, there is virtually no interaction between them. If we decrease the distance to a point at which the outermost orbitals start to overlap, however, chemical bonds begin to form between the atoms. At the same time, the discrete energy states start to split into multiple energy levels, eventually becoming near-continuous energy bands. At a distance characteristic for the crystal lattice of a given material, the energy bands might overlap or be separated by gaps of forbidden energies, the latter being the case for silicon.

Similarly to electron shells in a single atom, the energy bands are filled with electrons up to a certain point. If the last band that contains electrons is only partly filled, the respective material is a metal. Since electrons with the highest energies are within short reach of unoccupied energy states, they can move easily through the volume of the metal, making it a good conductor. On the other hand, when the last energy band that contains electrons is completely occupied, the respective material is either a semiconductor or an insulator. The deciding factor is the energetic distance between this band, known as the valence band, and the first empty band, known as the conduction band. This distance is the band gap, E_g , as shown in *Figure 2.3*.

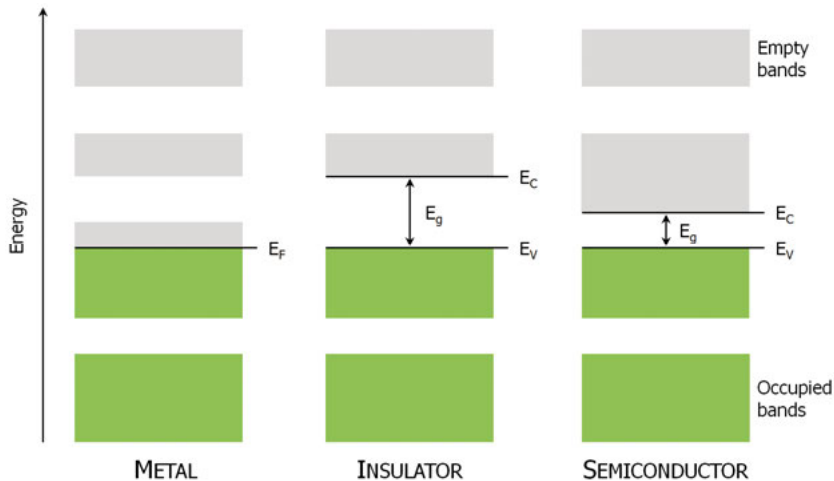


Figure 2.3. Energy bands of metals, insulators and semiconductors.

While band gap is one of the most important properties of any semiconductor, it is especially vital for solar cells materials. Different wavelengths of electromagnetic radiation correspond to different values of energy, and only photons of energy equal to or higher than the band gap can be absorbed in a given material. Moreover, depending on the crystal structure of a semiconductor, its band gap can be direct or indirect. The absorption process is more complex for materials with indirect band gaps, making them inferior light

absorbers, so direct band gaps are strongly preferred in photovoltaic applications.

Silicon

Silicon has an indirect band gap of 1.12 eV, which is lower than the optimum of around 1.4 eV for the solar radiation spectrum at Earth's surface [4], but still sufficient to produce conversion efficiencies of up to 26%. Since the band gap is indirect, the absorption coefficient is quite low, and layers of 200-300 μm are necessary to absorb all incident light. Despite not being the best absorber material, silicon is the most popular one. Its comparable simplicity, ubiquity in modern electronics, and the decades of extensive research on its properties, make it accessible and relatively cheap to produce.

CIGS

CIGS has a direct band gap that can be controlled by adjusting the $[\text{Ga}]/[\text{Ga}+\text{In}]$ ratio. The value changes from around 1 eV for pure CuInSe_2 to around 1.65 eV for pure CuGaSe_2 in an approximately linear fashion, and can be described by the following formula [5], in which x is the $[\text{Ga}]/[\text{Ga}+\text{In}]$ ratio.

$$E_g = 1.010 + 0.626x - 0.167x(1 - x) \quad (2.1)$$

This flexibility allows not only the tuning of the band gap to the optimal value of 1.38 eV, but also band gap grading, which can bring further improvements to device performance [6], and which was one of the subjects of **Paper II**. Since the band gap is direct, resulting in a high absorption coefficient, layer thickness of 2 μm or less is sufficient to absorb almost all incident light of energy equal to or higher than the band gap. Thus, CIGS is considered a thin-film solar cell material.

2.1.3 Free carriers

In the simplest scenario, each atom contributes a single valence electron to a covalent bond. Since the silicon atom has four valence electrons, it can form bonds with four of its neighbors. As the temperature increases from 0K, atoms begin to vibrate due to thermal energy, and some of the bonds may break. When that happens, the electrons involved in the bonds become free to move around the crystal lattice, leaving behind empty sites, known as holes. Holes are also free to travel through the crystal, but their movement is the result of multiple valence electrons swapping positions.

In energy terms, electrons are excited from the valence band to the conduction band, where they can easily move between the multitudes of empty energy states. Thus, they become free negative charge carriers. At the same

time, holes become corresponding positive charge carriers in the valence band. This process occurs continuously and is balanced by some of the electron and holes recombining to fix the broken bonds. Because the probability of thermal excitation increases with temperature, so do the populations of electrons, n , and holes, p . Consequently, contrary to metals, the conductivity of semiconductors also increases with temperature. In a steady state, the carrier populations in an intrinsic semiconductor are equal:

$$n = p = n_i \quad (2.2)$$

2.1.4 Carrier Transport – Drift and Diffusion

Once free carriers find themselves in their respective bands, there are two basic processes responsible for their transport: drift and diffusion. Both are illustrated in *Figure 2.4*.

Drift occurs in the presence of an electric field. Since electric field arises due to a potential difference, it is equivalent to an energy gradient, which creates a driving force for carriers. Electrons minimize their energy by moving towards lower potentials and holes by moving towards higher potentials. If the electric field becomes stronger, the energy difference grows and the carrier flow increases, resulting in a larger drift current.

Diffusion occurs when a gradient in concentration is present. Carriers with the same charge repel each other and are driven to spread evenly around the lowest available energy states. Higher concentration gradients lead to larger diffusion currents.

Both processes can occur simultaneously and often work against each other as a system tries to reach steady state.

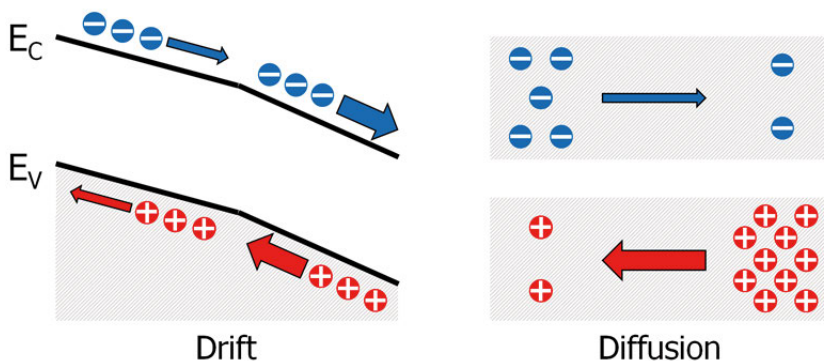


Figure 2.4. Basic transport mechanisms in semiconductors. Drift currents are driven by electric fields, while diffusion currents by differences in carrier concentrations. Stronger fields and larger concentration gradients give higher respective currents.

2.1.5 Recombination

Alongside the continuous carrier generation, recombination processes reducing the number of free carriers also occur. In general, these processes are the reverse of the generation process, which means that excess energy needs to be released by the recombining carriers. There are two main mechanisms through which this can happen: in radiative recombination the extra energy is released in the form of a photon, while in Auger recombination it is transferred to another conduction electron, which then thermalizes to the edge of the conduction band. Both these processes, illustrated in *Figure 2.5*, can occur with the assistance of defects located inside of the band gap.

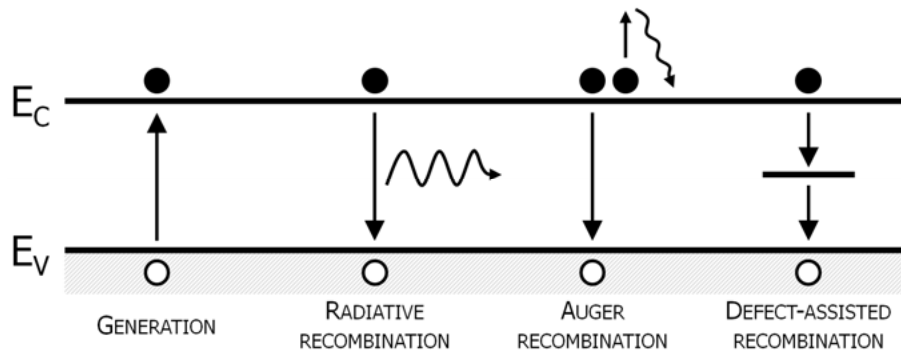


Figure 2.5. Schematic representation of carrier generation and different types of recombination in semiconductors.

2.1.6 Doping

Most often, intrinsic semiconductors are of little interest, since the relatively low carrier populations lead to high resistivity of intrinsic layers. Instead, the number of carriers of one type can be increased, and the resistivity decreased, by substituting some of the atoms of the original species with impurities that have different numbers of valence electrons. This process and the concentration of impurities are referred to as doping.

Silicon

Let us imagine that one of the atoms in a silicon crystal is replaced by a dopant atom with five valence electrons. As long as the energy of the surplus electron is relatively close to the edge of the conduction band, a small amount of thermal energy is enough to excite the electron to the conduction band where it becomes a free carrier. On the other hand, if the substitute atom has three valence electrons, and the energy required to add the missing electron is sufficiently close to the edge of the valence band, valence electrons from neighboring atoms can be excited to this energy state, releasing a free hole to the valence band. The more impurities are introduced, the more

the population of free electrons or holes increases. When the number of ionized dopants significantly exceeds the intrinsic carrier concentration, the doping is referred to as *n*-type or *p*-type if the majority carriers are respectively electrons or holes. The most common doping method for silicon is ion implantation, which relies on bombarding silicon layers with high energy ions of the desired dopant. As a result, the doping process can be finely controlled to achieve the required doping profiles.

CIGS

While in silicon doping is usually an intentional process, CIGS layers grown under most conditions are naturally *p*-type due to intrinsic defects [7]. In fact, obtaining *n*-type CIGS layers is difficult and demands specific growth conditions [8], [9].

The chief acceptor dopant is the copper vacancy, V_{Cu}^- , which exhibits very low formation energies even at Cu-rich conditions, and thus can be found in most CIGS layers in concentrations of 10^{20} - 10^{21} cm^{-3} [8], [9]. The fact that an atom vacancy can be negatively charged might be somewhat confusing, but the explanation is rather simple. With the copper atom missing, the lattice around its site relaxes a little, and the neighboring atoms can share the electrons from their broken bonds to form a new pair of bonds between them instead. Since one of the electrons is missing together with the copper atom, a free electron needs to be captured to complete the process, giving the vacancy a negative charge.

Although the net doping in CIGS is of *p*-type, large numbers of donor defects are also present in CIGS layers, making them highly compensated. In_{Cu}^{2+} and Ga_{Cu}^{2+} substitutional defects can be found in concentrations similar to V_{Cu}^- , resulting in a net doping of only 10^{14} - 10^{16} cm^{-3} .

Theoretical calculations predict that many of these defects can form defect complexes such as $(In_{Cu}-2V_{Cu})$, which have unusual electrical properties [10], [11]. Some of the impact the intrinsic defects in CIGS can have on electrical behavior will be discussed in more detail in section 5.

2.1.7 Fermi Level

The probability that a state of energy E is occupied by an electron is given by the Fermi-Dirac distribution.

$$f(E) = \frac{1}{1 + \exp[(E - E_F)/kT]} \quad (2.3)$$

At 0K, the Fermi-Dirac distribution is equal to zero for energies higher than E_F , and equal to one for energies equal to or lower than E_F . Thus, E_F represents the highest occupied energy level, known as the Fermi level. Above

0K, the Fermi-Dirac distribution becomes more gradual with increasing temperature, but continues to be centered on the Fermi level, which now represents the energy level with 50% probability of being occupied.

In practice, E_F is related to the concentration and the average energy of free carriers. Consequently, in intrinsic semiconductors, in which there is a balance between free electrons and free holes, E_F lies close to the middle of the band gap. In non-degenerate doped semiconductors, E_F lies between the band gap and edge of the band corresponding to the majority carrier type, as depicted in *Figure 2.6*.

The concept of a single, continuous Fermi level is only valid for systems in thermal equilibrium. As soon as additional carriers are introduced into a system due to external factors, such as voltage-controlled carrier injection, the Fermi level can no longer represent the balance between electrons and holes. While in such cases there is no equilibrium between the conduction and valence bands, carriers within the bands can still reach *local* equilibria as long as the system is in a steady state. Thus, it is possible to describe each carrier population separately using *quasi*-Fermi levels, E_{Fn} and E_{Fp} . These quantities allow reasonably simple mathematical descriptions of semiconductor systems to continue in non-equilibrium scenarios.

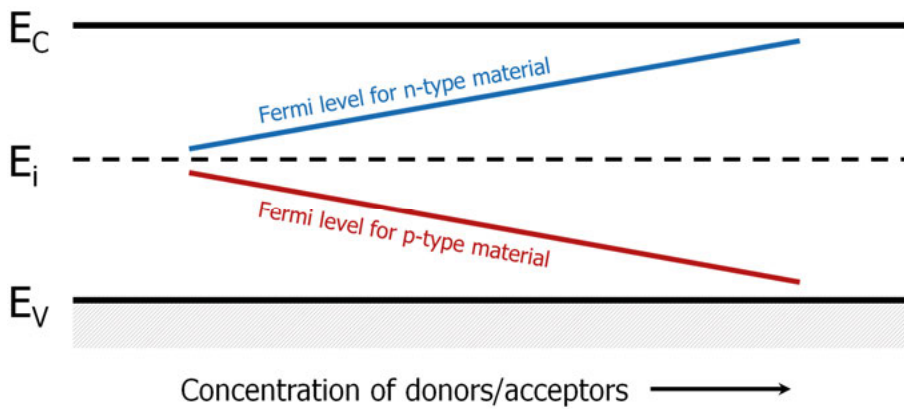


Figure 2.6. Fermi level position versus concentration of donors or acceptors.

2.2 p - n Junctions

A p - n junction is formed when a p -doped semiconductor layer is in contact with an n -doped layer. It is one of the simplest semiconductor devices, often used as a building block in more complex ones. It also forms the basis for most solar cell designs.

2.2.1 Depleted Layer and Built-In Potential

A semiconductor device reaches thermal equilibrium when the Fermi level is constant throughout it. Initially, the Fermi level is at different positions on the two sides of a p - n junction because of different carrier concentrations. Thus, some of the electrons from the n side start to diffuse to the p side, and an equivalent process occurs for the holes from the p side. Since part of the ionized donors and acceptors closest to the interface between the two materials are no longer neutralized by the corresponding free carrier populations, their static charge gives rise to an electric field. The field acts against the diffusion process, repelling majority carriers from the interface region. This part of the junction becomes almost completely devoid of free carriers, and is known as the depleted layer or the space charge region, as illustrated in *Figure 2.7*.

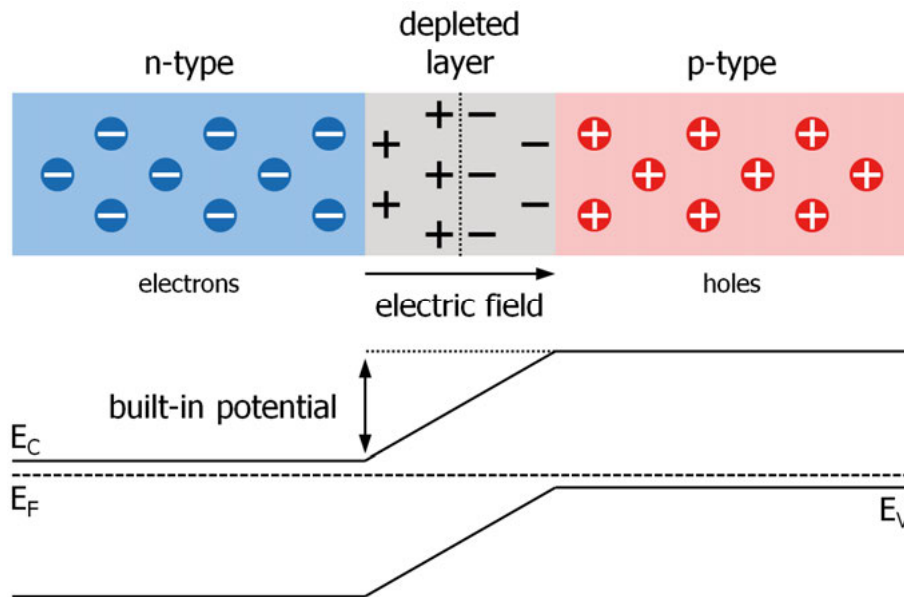


Figure 2.7. Distribution of charge in a p - n junction and the corresponding schematic band diagram in equilibrium. The absence of free carriers in the depleted layer gives rise to an electric field due to uncompensated ionized dopants on both sides of the junction. In turn, the field repels majority carriers from the depleted layer.

The presence of electric field is represented graphically as bending of the energy bands. The difference in energy between the two sides of the p - n junction in thermal equilibrium is defined as the built-in potential. Its magnitude depends on the concentrations of donors on the n -side and acceptors on the p -side, together with the intrinsic carrier concentration of a given semiconductor. Thus, highly-doped junctions are usually characterized by a large built-in potential.

2.2.2 Current-Voltage Characteristics

When a small positive voltage bias is applied to a p - n junction in such a fashion that the n -side is kept at zero potential, it means that the p -side is at a small positive potential. As a result, the built-in potential decreases by the applied voltage (multiplied by the elementary charge) and more electrons (holes) from the n -side (p -side) of the junction can diffuse to the p -side (n -side). The balance between drift and diffusion currents no longer holds as the diffusion current starts to dominate. As the bias increases, the number of carriers diffusing over the junction grows exponentially, with the total current density is given by the Shockley equation.

$$J = J_0 \left[\exp\left(\frac{qV}{kT}\right) - 1 \right] \quad (2.4)$$

J_0 is known as the reverse saturation current density and is one of the parameters that represent the quality of a p - n junction. Its value corresponds to the largest amount of current that can flow through the junction in reverse direction, and is typically multiple orders of magnitude lower than those of forward currents during device operation. When a small negative voltage bias is applied to a junction, the reverse current quickly increases to J_0 , after which it stays constant with increasing bias. The negative potential attracts electrons to the n -side, and holes to the p -side, but since almost all of them are already on their respective sides of the junction, there are virtually no carriers to support current flow.

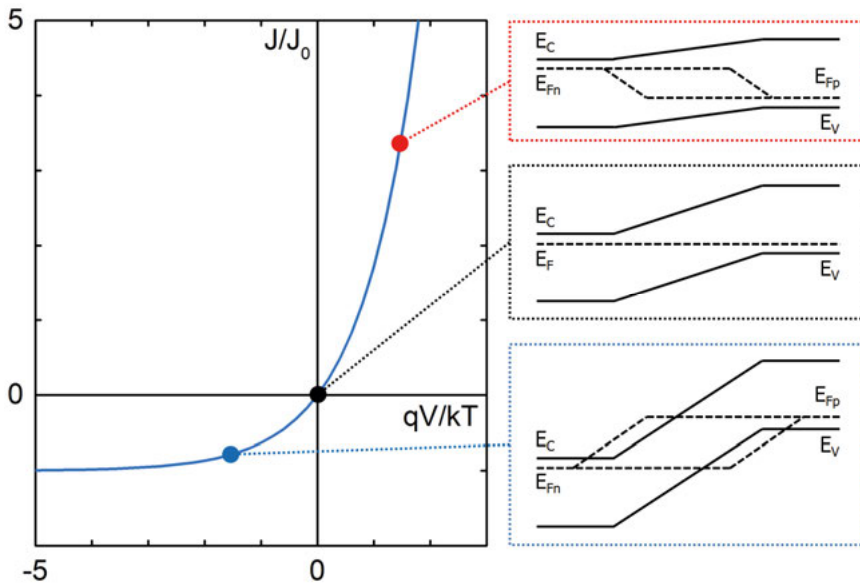


Figure 2.8. Current-voltage characteristics of an ideal p - n junction with band diagrams corresponding to reverse, zero, and forward bias.

Because a junction under forward or reverse bias is no longer in thermal equilibrium, carrier populations need to be described using the quasi-Fermi levels, and the distance between them is equal to the applied voltage. This is illustrated in *Figure 2.8* together with a plot of the current-voltage (IV) characteristics of an ideal p - n junction.

2.2.3 Homo- and Heterojunctions

The simplest type of p - n junction, homojunction, is formed when both sides of the junction are made of the same semiconductor material. The energy bands bend on both sides of the depleted layer, but are joined smoothly at the interface. This is rarely the case in heterojunctions, in which the two sides of the junction are formed from different semiconductor materials. Dissimilar semiconductors can not only have different band gaps, but also electron affinities and work functions. This means that there are usually discontinuities at the points at which the energy bands of the two sides of a heterojunction meet. The difference in electron affinities, which represent the energetic distance of the conduction band edge from the absolute vacuum level, defines the magnitude of the discontinuity in the conduction band edge. Together with the band gaps and the work functions, they determine if the nature of the discontinuity is a spike or a cliff.

Silicon

Silicon-based solar cells are typically homojunctions with a lightly-doped p -type absorber layer and a very thin strongly-doped n -type emitter layer, which takes its name from the classic bipolar transistor terminology.

CIGS

CIGS solar cells utilize multi-layer heterojunctions, with p -type CIGS as the absorber layer, CdS or a Cd-free alternative as the immediate n -type buffer layer, followed by a semi-metallic n -type transparent conducting oxide ZnO:Al. As mentioned before, the band gap of the CIGS layer can be varied between around 1 eV and 1.65 eV by adjusting the [Ga]/[Ga+In] ratio from zero to one. Assuming the use of a CdS buffer, the conduction band discontinuity between the buffer and the absorber goes from a large spike for a CIS/CdS interface to a large cliff for a CGS/CdS interface. Since large spikes have current-blocking properties and cliffs tend to increase interface recombination, neither is desired in solar cell applications. Consequently, the best devices are obtained for compositions resulting in no discontinuities or in small spikes [12]. A schematic band diagram for CIGS devices is presented in *Figure 2.9*.

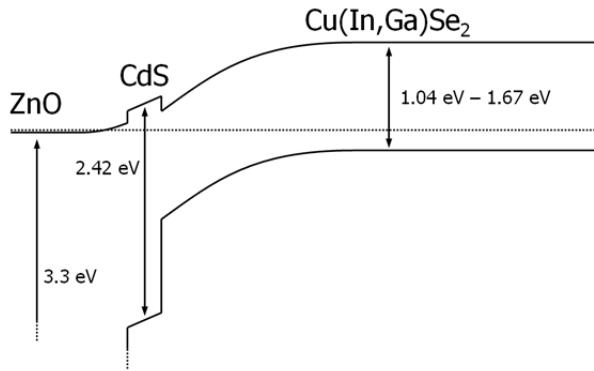


Figure 2.9. Schematic band diagram for CIGS devices. As the band gap of CIGS increases with growing $[\text{Ga}]/[\text{Ga}+\text{In}]$ ratio, the spike at the CdS/CIGS interface decreases and eventually becomes a cliff.

2.2.4 Junction Breakdown

When a p - n junction is exposed to a sufficiently high reverse bias, the electric field might reach a critical value, leading to junction breakdown. In this state, the junction no longer has blocking properties in the reverse direction, and instead conducts a very large current. There are three main breakdown mechanisms: thermal runaway, avalanche multiplication, and tunneling.

Thermal breakdown occurs at high reverse bias when the combination of voltage and current generates enough power in a device to cause heat dissipation that exceeds its cooling capacity. The resulting increase in temperature leads in turn to an increase in the reverse current, creating a positive feedback loop that can ultimately destroy the device.

Avalanche breakdown occurs when the electric field in the device can accelerate the free carriers to energies sufficient for impact ionization, which generates additional electron-hole pairs and continues in an avalanche fashion. Avalanche breakdown usually results in more gradual breakdown curves than tunneling breakdown, and is characterized by a positive temperature coefficient, i.e. the breakdown voltage increases with increasing temperature. The reason for this is that at higher temperatures the carriers are more likely to lose some of their energy through scattering because of increased crystal lattice vibrations.

Tunneling breakdown occurs in highly-doped junctions when the electric field makes the energy bands in the depleted layer steep enough to allow band-to-band tunneling. The process is effectively tunneling through a triangular potential barrier, with the barrier height given by the band gap. Consequently, it has a negative temperature coefficient, as the band gaps of most semiconductors decrease with increasing temperature. Breakdown curves produced by tunneling breakdowns are sharper than those of avalanche breakdowns, usually with well-defined breakdown voltages.

Junction breakdown in CIGS solar cells is the subject of **Papers I** and **IV**. **Paper I** shows that its behavior does not easily fit into any of the breakdown types discussed above. Instead, it might be a combination of avalanching and tunneling, further complicated by the involvement of intrinsic defects. Moreover, its character changes in the presence of blue illumination. In **Paper IV** we propose a model explaining the behavior of breakdowns measured in darkness. Despite the effort put into the analysis, the complexity of the problem was a major obstacle to extending the model to breakdowns measured under blue illumination. Further discussion follows in section 5.3.

2.3 Solar Cells

In darkness, most solar cells are ordinary p - n diodes, and can be described by the corresponding physics. In this part of the chapter, we will focus on the photovoltaic effect, and how it makes illuminated solar cells more than simple diodes.

2.3.1 Solar Radiation Spectrum

The solar spectrum covers a small range of electromagnetic radiation, from near-ultraviolet to near-infrared, as shown in *Figure 2.10* [13]. The visual spectrum is only a small subset of that range in turn, although it does contain a significant fraction of available photons. Typically, solar cells are characterized and certified at 25°C, using the AM1.5 spectrum with an intensity of 1000 W/m², which is a reasonable approximation of the average conditions that solar cells might operate in in most climates. This set of conditions is referred to as the standard test conditions (STC). The AM1.5 spectrum accounts for the changing position of the sun by assuming a tilt of 37°, and for the partial absorption of light by chemical species present in the atmosphere.

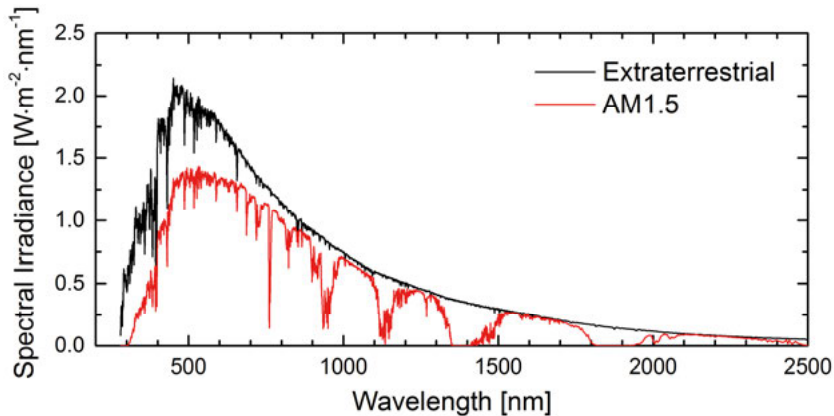


Figure 2.10. Solar spectrum outside of Earth's atmosphere and at its surface.

2.3.2 Absorption of Light

As described in section 2.1.2, the band gap is the main semiconductor property which determines the likelihood of light absorption. When a photon is absorbed in a semiconductor, its energy is spent exciting a valence electron to the conduction band, as illustrated in *Figure 2.11*. Since there are no energy states inside of the band gap in a defect-free material, it imposes a lower limit on the energy required for absorption equal to the band gap value. In indirect-band-gap semiconductors, the excitation process must be accompanied by a change in electron momentum, which requires the participation of organized lattice vibrations known as phonons. As a result, absorption becomes a three-particle process, and its probability is decreased in comparison to direct-band-gap semiconductors, in which it is a matter of interaction only between photons and electrons. In some cases, exceptions to the three-particle requirement are possible if high-energy states for which momentum can be preserved exist above the conduction band edge, provided that incident photons have enough energy for such excitation.

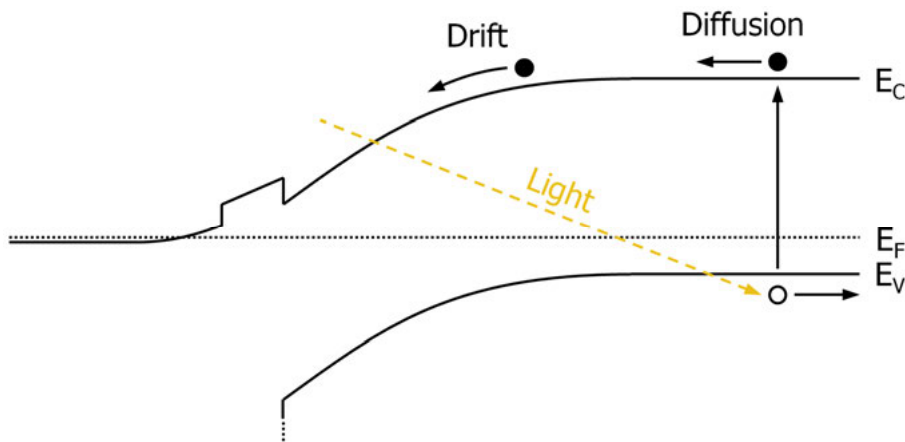


Figure 2.11. Light absorption and carrier generation, followed by carrier transport.

2.3.3 The Photovoltaic Effect and Photocurrent Generation

In practice, a typical solar cell with a p -type absorber illuminated with the AM1.5 spectrum generates around 10^{17} electron-hole pairs per second for every cm^2 of its area. While this rate of generation does not have a significant impact on the concentration of holes, the number of electrons in the conduction band increases by many orders of magnitude. Thus, the system is no longer in thermal equilibrium and the Fermi level splits on both sides of the junction. To extract current from the solar cell, the electron-hole pairs need to be separated and the electrons must reach the n -side of the junction. The latter is a two-step process for electrons generated outside of the

space-charge region of the absorber layer. First, they must diffuse through the neutral bulk to the edge of the space-charge region, after which they can be collected by the electric field and swept to the n -side. If no external terminals are connected to the solar cell, the majority carriers will start to pool on their respective sides of the junction. Consequently, a voltage drop will arise over the junction, counteracting the collection process by increasing the forward diffusion current. Once steady state conditions are reached, drift and diffusion components cancel each other out, just like in thermal equilibrium. The voltage drop is equal to the difference in majority-carrier quasi-Fermi levels on the two sides of the junction, and is known as the open-circuit voltage.

2.3.4 Current-Voltage Characteristics and Efficiency

For an ideal solar cell, the Shockley equation (2.4) gains an additional term which corresponds to the light-generated current density, J_L .

$$J = J_0 \left[\exp \left(\frac{qV}{kT} \right) - 1 \right] - J_L \quad (2.5)$$

Since the photocurrent flows in the opposite direction to the forward diode current, it is typically represented as negative. Thus, the current-voltage (further referred to as IV) characteristic of the solar cell under illumination shifts down by the value of J_L , as shown in *Figure 2.12*.

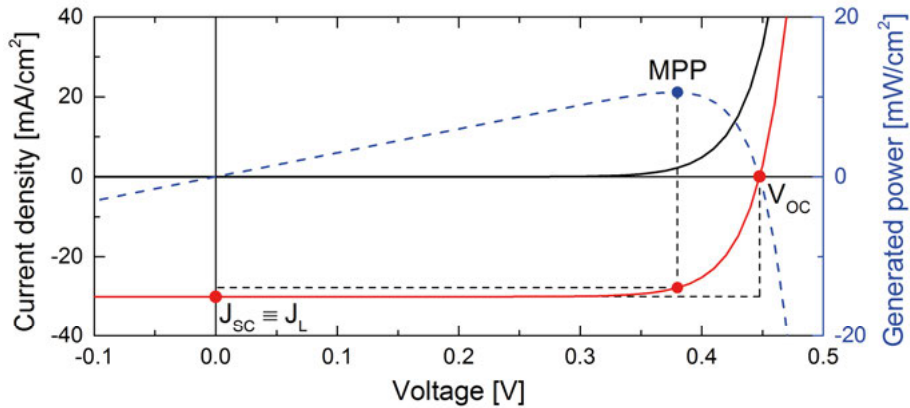


Figure 2.12. Example current-voltage characteristics of an ideal solar cell. The dashed blue line shows the power profile with the maximum power point (MPP) marked by the blue dot.

Several useful parameters can be extracted from light IV characteristics. The voltage measured at the point at which no current flows through the device is the already discussed open-circuit voltage, V_{oc} . The current measured at 0V is the photocurrent, otherwise known as the short-circuit current, J_{sc} . By

plotting the product of current and voltage, the maximum power point can be found, which gives the values of V_{mp} and J_{mp} . Together, these four parameters determine the fill factor, FF , of the device.

$$FF = \frac{V_{mp} \cdot J_{mp}}{V_{oc} \cdot J_{sc}} \quad (2.6)$$

It is a measure of how rectangular the light IV curve is. While values of above 0.8 are often achieved in silicon solar cells, in CIGS devices they usually stay below this level. In well-behaved devices, fill factor is related to the energy-conversion efficiency, η , of a solar cell through the following relationship.

$$\eta = \frac{V_{mp} \cdot J_{mp}}{P_{in}} = \frac{V_{oc} \cdot J_{sc} \cdot FF}{P_{in}} \quad (2.7)$$

P_{in} is the total power of the light incident of the device, equal to 1000 W/m^2 in standard test conditions. The energy-conversion efficiency, usually referred to simply as efficiency, is the most important solar cell parameter in practical applications. While complex multi-junction devices have reached small-scale efficiencies above 40%, single-junction cells are limited by a theoretical barrier of just below 30%, and most commercially-available modules have efficiencies closer to 15%. The reason is that real-world devices are in most cases far from ideal, and there are many factors which contribute to the lowering of efficiency.

The IV characteristics of non-ideal solar cells can be much more complex than those of ideal devices. Voltage-dependent current collection and secondary barriers [14] can cause the behavior of dark and illuminated IV characteristics to differ. Moreover, the value of FF can be deceiving in reflecting the nature of some IV curves. If an IV characteristic is a straight line beginning at J_{sc} and ending at V_{oc} , its FF will be equal to 0.25 regardless of the values of these parameters. Additionally, certain deformations in IV curves can result in multiple maximum power points, rendering FF meaningless. CIGS solar cells in particular are well-known for a plethora of such effects, some of which are the subject of **Paper III**. More details on this topic can be found in section 5.

2.3.5 Power Losses

We will now consider the different sources of losses present in solar cells, from the moment illumination reaches the surface of a device to the extraction of current into an external circuit.

Shading

Let us consider a simple statement: shaded solar cells cannot generate electricity. The obvious solution to this issue is to place solar panels in a fashion that minimizes, if not eliminates, the amount of shading from neighboring objects: trees, chimneys, other solar panels, etc. But there is also another source of shading losses. Most solar cell designs include metallic grids deposited on top of the device, which assist current collection from the transparent conducting layers serving as front contacts. While these grids are typically very thin, they still cover between 2 to 3 percent of active area, effectively reducing the amount of incident light. Because of that, when electrical performance is in focus, efficiency values are sometimes given per unit of active area.

Reflection

Since the surface of a solar cell marks the boundary between two mediums with different refractive indices, some of the incident light can be reflected from the surface instead of being transmitted. This is especially true for high incidence angles. Thus, commercially-available modules often use antireflective coatings which reduce reflective losses through better-matched refractive indices. Another solution is surface-patterning of the topmost layers, often into pyramid-like shapes, which causes light scattering and decreases reflection probability.

Parasitic Absorption

Photons that penetrate into the solar cell need to reach the absorber layer to generate useful electron-hole pairs. If they are absorbed before that, it is considered parasitic absorption, because the extremely short minority-carrier lifetime in the highly doped front layers makes collection very unlikely.

A significant part of the solar spectrum is lost to parasitic absorption in CIGS solar cells with CdS buffer layers. CdS has a direct band gap of 2.42 eV, which means it can absorb photons of wavelengths equal to and lower than 512 nm. Coupled with the fact that cadmium is a toxic element, efforts are made to find replacement buffer layers with wider band gaps [15], [16]. Substituting CdS with alternative buffers can yield an increase in photocurrent due to reduced parasitic absorption in the spectral range of 350-550 nm. This will be further discussed in section 3.4.

Generation and Thermalization Losses

Once photons reach the absorber layer, they can be absorbed if their energy is equal to or higher than the band gap. Consequently, low band gap materials can generate higher photocurrents, which could suggest that they make superior absorbers. However, there is another side to absorption that we have not considered yet. When absorbed photons have more energy than the size

of the band gap, they excite carriers into higher energy states in their respective bands. The excess energy is then lost to the crystal lattice as carriers relax to the edge of the conduction band in a process called thermalization. Additionally, a single photon can only create a single electron-hole pair, even if its energy is a multiple of the band gap energy. These energy losses are realized in the fact that open-circuit voltage is limited by the degree of quasi-Fermi level splitting, which in turn cannot exceed beyond the confines of the band gap. Thus, while low band gap absorbers generate higher currents, high band gap absorbers generate higher voltages. The tradeoff means that there is an optimal band gap which maximizes power output. For the AM1.5 spectrum this optimum is at 1.4 eV [4]. It is worth noting that generation and thermalization losses are by far the strongest factors limiting conversion efficiency. Even at the optimal band gap, they constitute more than half of the energy available in the solar spectrum.

Recombination

Carrier recombination is another factor that significantly contributes to decreased performance of solar cell devices. Since photogenerated electrons and holes are non-equilibrium carriers, recombination processes are a natural way of restoring equilibrium. In section 2.1.5 different recombination mechanisms were described, and now we can define three main recombination *paths* based on the affected region of the device: interface, bulk, and back contact.

In good quality solar cells, recombination occurs mainly through defects in the neutral bulk, where illumination generates many minority carriers and no field is present to drive them away from the majority carriers. This is in contrast with textbook descriptions of recombination in unilluminated diodes, in which usually very few minority carriers reach the neutral bulk even under forward bias. Consequently, recombination is most effective in the space-charge region, where the Fermi level crosses the middle of the band gap and carrier populations are close to equal. In practice, the region in which recombination dominates depends on the character of the defects present in a given device. Therefore, in some solar cells, recombination in the space-charge region rather than in the bulk might indeed dominate.

Interface recombination is especially undesirable in photovoltaic devices, since it can be particularly detrimental for open-circuit voltage. This is because V_{oc} strongly depends on the hole barrier at the interface, which is the difference between the edge of the valence band and the electron quasi-Fermi level.

Recombination at the back contact can also negatively affect device performance, but is usually not an issue, since many cell designs utilize some form of an electron-repelling back-surface field. In CIGS solar cells it arises spontaneously when MoSe_2 is formed at the back contact during absorber

deposition [17], although band-gap-grading can also be used to further enhance the back-surface field [6].

The main recombination mechanism can be determined experimentally [18], although with a limited degree of confidence [19], [20]. Moreover, in CIGS devices, recombination profiles can be significantly affected by some treatments involving illumination and voltage bias [21], [22]. One example is the red-on-bias effect [23] explored in **Paper III**.

Series and Shunt Resistance

When current flows through a semiconductor, it encounters electrical resistance, which is a function of layer dimensions, carrier mobility, and carrier concentration. Each layer in a solar cell, along with the contacts, contributes to the total series resistance of the device, lowering the voltage drop over the junction and limiting the current that can freely flow through the device.

At the same time, in addition to the main current path, *additional* paths might exist, through which some of the current can flow. This results in loss of the photogenerated current, and is detrimental to device performance. In practical terms, the contribution from all such unwanted currents paths can be represented as a parallel resistance, often referred to as shunt resistance.

In the best case scenario, series resistance should be minimized, while shunt resistance should be kept as high as possible. In reality, this is relatively easy to achieve in small-scale devices, but poses a more serious issue in large-scale modules. In CIGS solar cells, the two types of resistance can be affected by external conditions. Driving large currents through a device, such as under breakdown, causes a lot of heat dissipation, which can burn conductive paths into the device, decreasing shunt resistance [24]. On the other hand, some materials exhibit photoconductivity, which results in a decrease of series resistance under illumination. This last effect might be behind the difference in breakdown behavior of CIGS devices measured in darkness and under blue illumination, which is a topic explored in **Paper I** and **Paper IV**. Moreover, the impact of series and shunt resistance was important in modelling of breakdown currents in **Paper IV**.

2.3.6 The One-Diode Model

The one diode model is an attempt to represent the non-ideal solar cell as a simplified electrical circuit, as illustrated in *Figure 2.13*. Equation (2.5) can be further modified to include series resistance R_s , shunt resistance R_p , and the contribution of recombination, in the form of the ideality factor n .

$$J = J_0 \left[\exp \left(\frac{q(V - JR_s)}{nkT} \right) - 1 \right] + \frac{V - JR_s}{R_p} - J_L \quad (2.8)$$

The resulting formula can be transformed into an equivalent electrical circuit shown in *Figure 2.13*. The one-diode parameters can be extracted from IV measurements by fitting the experimental curves with equation (2.8). This usually works fine for well-behaved samples, but fails in more complex scenarios, such as those discussed in **Paper III**. In most cases, however, the values of J_0 and n provide useful information about recombination in the measured device.

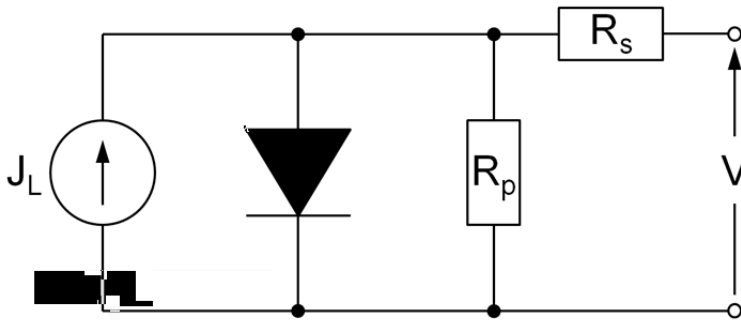


Figure 2.13. Equivalent circuit of a solar cell.

3. Cu(In,Ga)Se₂ – Device Structure

The most common CIGS solar cell design involves sequential deposition of layers in a substrate configuration, starting with the back contact, as shown in *Figure 3.1*. In this chapter, I will give short descriptions of each layer and the corresponding deposition processes, accompanied by some remarks relevant to the included papers.

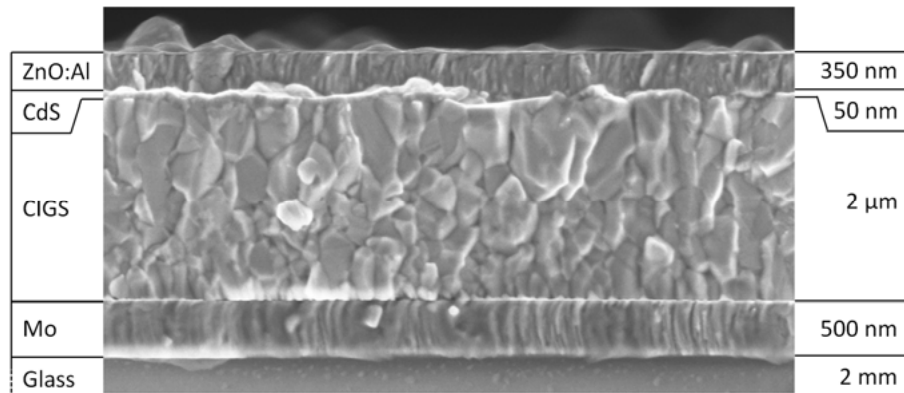


Figure 3.1. Scanning electron microscopy image of a CIGS device, with layer types marked on the left side and typical layer thickness on the right side.

3.1 Substrate – Soda-Lime Glass

Most CIGS devices use 1-to-3-mm-thick soda-lime glass (SLG) as the substrate, which is relatively cheap and which functions as an uncontrolled sodium source. The role of sodium in CIGS films has been one of the most hotly debated topics in the CIGS community since the discovery of its beneficial impact on device performance [25]. Multiple studies have been made on the subject, both theoretical [26] and experimental [27]–[29]. If no barrier for sodium diffusion is deposited on top of the SLG substrate, some electrical grounding schemes of the modules in a system might lead to excess sodium migration into the active layers during device operation. This effect can be extremely detrimental to module performance, and is known as potential-induced degradation (PID) [30], [31]. Diffusion barriers not only protect against PID, but combined with sodium-based precursor layers, such as NaF,

also allow more control over the amount of Na incorporated into the grown films.

3.2 Back Contact – Mo

A layer of molybdenum with a thickness of around $0.5\ \mu\text{m}$ is usually sputtered on top of the SLG substrate as the back contact. During CIGS deposition, part of the Mo layer is consumed in a selenization process, forming a thin film of MoSe_2 [17], [32]–[34]. The formation of this additional layer is benevolent for device performance, resulting in an ohmic-type contact between the CIGS absorber and the Mo layer [17], [34], [35]. Typical sheet resistance of the Mo back contact is in the order of $1\ \Omega/\square$ [36].

3.3 Absorber Layer – CIGS

As described in section 2.1.2, CIGS has a variable band gap, which can be controlled by the $[\text{Ga}]/[\text{Ga}+\text{In}]$ ratio. Most of the high efficiency devices have been produced using co-evaporation deposition [3], including the current record-holder cell with an efficiency of 22.6% [2]. In this approach, the individual elements are evaporated from their respective sources onto the SLG substrate, typically heated to $500\text{--}550\ ^\circ\text{C}$ [36]. The resulting films are *polycrystalline*, with a typical thickness of $1.5\text{--}2.5\ \mu\text{m}$, and grain dimensions in the range of $1\ \mu\text{m}$. Unlike the grain boundaries in many other materials, those in polycrystalline CIGS were found to have a benign nature [37]–[40]. High substrate temperature facilitates the growth of high-quality CIGS layers with increased grain size and improved performance, but increases the cost of deposition and limits the choice substrates [41]–[43]. While CIGS films are usually grown Cu-poor, with a $[\text{Cu}]/[\text{Ga}+\text{In}]$ ratio of around 0.8 to 0.9, the material shows remarkable tolerance to a wide window of compositions [44]. This was also shown in **Paper II**, which explores the effects of extreme copper variations on material properties and performance of CIGS solar cells.

3.3.1 Band-gap Grading

The elemental fluxes from the evaporation sources can be varied over time to alter the distribution of elements in the deposited layers. Consequently, many different deposition processes have been proposed, some with multiple stages that employ different evaporation rates or use only a subset of the elements. One popular process is the three-stage process, first presented in [45] and then successively improved, producing many record-breaking devices over the years [46], [47]. The resulting films have characteristic

[Ga]/[Ga+In] profiles, with the band gap decreasing towards the front of the CIGS layer, finished with a small ‘notch’ as it slightly increases again. While the benefits of band-gap-grading have been a subject of debate [48], [49], it is commonly used in one form or another [50]. The simplest approach is to have a single linear gradient throughout the CIGS layer, which is easy to obtain in in-line deposition systems [36]. Such samples and the impact of Cu content on their grading were investigated in **Paper II**.

3.4 Buffer Layers – CdS and Cd-free Buffers

The *n*-side of the heterojunction comprises of three different layers, beginning with the buffer, which determines interface properties and protects the interface region from damage caused by sputtering of the subsequent layers. While many different buffers have been tested over the years [15], [16], the most successful material to fill that role continues to be CdS, as evidenced by its usage in almost all record-breaking cells. A notable departure from its domination was shown recently by the record-level devices employing different combinations of (Zn,Mg)O and Zn(O,S,OH) layers in the buffer role [51], but this marks more of an exception than a rule.

The impact of various buffer layers on some of the electrical phenomena present in CIGS solar cells was explored in **Paper I**, **Paper III**, and **Paper IV**.

3.4.1 CdS

CdS is usually deposited in a wet process known as chemical bath deposition. After Mo and CIGS layers are finished, the processed devices are immersed in a liquid solution of ammonia, thiourea, and a cadmium salt, which is heated and stirred, either periodically or continuously. The resulting films give a very conformal coating [52], and the typical thickness is around 50 nm. Good surface coverage is not the only advantage of CdS, as the chemical bath also etches the surface removing unwanted oxides [53], while Cd atoms can diffuse into the surface region of the CIGS layer, possibly acting as *n*-type dopants and facilitating type inversion [54]–[56]. Unfortunately, Cd and other chemicals used in the deposition of CdS layers are highly toxic, spurring research into alternative buffers. Another drawback of CdS is its relatively low band gap of 2.42 eV, which causes significant parasitic absorption. CdS thickness was one of the device parameters investigated in **Paper I** and **Paper IV**. The red-on-bias effect studied in **Paper III** is strongest in samples with CdS buffers.

3.4.2 $\text{Zn}(\text{O,S})$ and $\text{Zn}_x\text{Sn}_{1-x}\text{O}_y$

Both $\text{Zn}(\text{O,S})$ [57], [58] and $\text{Zn}_x\text{Sn}_{1-x}\text{O}_y$ (ZTO) [59] are chemical cousins of ZnO , and can be used as alternative buffers in CIGS solar cells. Not only are they more environmentally friendly substitutes for CdS , but also offer better optical properties due to higher band gaps of 3 eV or more. Moreover, tuning the ratio between O and S in $\text{Zn}(\text{O,S})$ [60] or Zn and Sn in ZTO [61] allows control over the band gap and optimization of the conduction band offset. In ZTO layers this can be also achieved through changes in deposition temperature [62]. Both materials can be grown using atomic layer deposition, which is a slow chemical process that produces very conformal high-quality layers. Breakdown properties of samples with different ZTO thicknesses from reference [63] were investigated in **Paper I** and **Paper IV**. One of the conclusions was that ZTO layers provide much better protection from high reverse currents than CdS . In **Paper III**, metastable behavior of samples with both types of alternative buffers was compared with that of CdS -based samples.

3.5 Front Contact – i- ZnO and ZnO:Al

The topmost layer of most CIGS devices is the window, which is responsible for lateral transport of current. Thus, it needs to offer excellent conductivity, but stay highly transparent to minimize parasitic absorption. One of the most commonly used materials in that role is degenerately aluminum-doped ZnO with a direct band gap of 3.3 eV, although it is only one of many different transparent conducting oxides used in photovoltaics [64]. ZnO:Al layers are usually deposited through sputtering, with a typical thickness of around 500 nm and sheet resistance in the order of $30 \Omega/\square$ [36]. While the resistance can be lowered by increasing film thickness, the benefits are offset by decreasing layer transparency. A thin film of more resistive intrinsic ZnO is usually deposited before the doped layer to minimize the effect of locally inhomogeneous electronic quality [65]. The thickness of this layer is typically around 100 nm.

4. Electrical Characterization of CIGS Solar Cells

4.1 The ICVT Setup

My main companion in electrical characterization of CIGS solar cells was the ICVT setup. The name is an abbreviation: I for current, C for capacitance, V for voltage, and T for temperature. The ICVT setup began its life as a cryostate-based setup for temperature-dependent IV characterization, but grew into a much more advanced system. In the first year of my PhD studies, we streamlined its construction, added an LCR (inductance, capacitance, resistance) meter, and replaced the original halogen lamp with an array of diodes providing different colors of illumination.

The heart of the system is a liquid-nitrogen-cooled cryostate with a 5 cm x 5 cm copper sample stage. For temperature-dependent measurements, samples need to be affixed to the stage with thermal glue to provide good contact. Interestingly, one of the best products that can be used in this role is a glue for artists called Fixogum, since it offers excellent thermal conductivity even at temperatures as low as 35 K [66]. That is more than enough to cover the range of temperatures available with liquid nitrogen cooling, which allows a minimum sample-stage temperature of around 81 K. Due to poor thermal conductivity of soda-lime glass, several minutes are needed to stabilize sample temperature, and the time required depends on glass thickness. The temperature of the sample stage is controlled with a Lakeshore 330 Autotuning Temperature Controller. Since the autotuning is not always reliable, I found a set of PID (proportional-integral-derivative) parameters that works for the intended temperature range of 100 K to 360 K. With these parameters (the exact values are of less importance), the amplitude of the temperature variation could be kept below 1 K.

Mounted on the sample stage are two probes with two tips each in a four-point configuration for contacting of the samples. In this configuration, current and voltage are measured in separate circuits, and the effect of wire and contact resistances on the measured voltage is almost completely eliminated. Reference [67] has a very nice example of how much a measurement of MOSFET drain current can be affected by contact resistance if a four-point probe setup is not used. The four wires are connected to a com-

puter-controlled switchbox, which is programmed to automatically choose the instrument relevant to a given measurement.

The first of the two choices is a Keithley 2401 source-measure unit. This instrument is used for different types of current-related measurements. One important function of the meter is the setting of compliance, which is the maximum current allowed to flow through the measured device. Since the open-circuit voltage in different CIGS samples can vary by as much as 300-400 mV, a given forward voltage might result in small current in one case or a device-killing current in another. A reasonable current compliance will prevent damage in the latter case by limiting the voltage and the current. Another instrument feature worth a comment is the built-in voltage or current sweep. While it is possible to sweep either of these parameters by sending commands corresponding to individual values of voltage or current, the sweep function offered by the instrument is much faster, which might be a significant factor in some measurement scenarios, e.g. breakdown measurements. The measurement process can also be sped up by setting the number of power line cycles over which the instrument integrates to less than one. This decreases the accuracy of measuring very small currents, but makes the measurement significantly faster. I used this approach for some breakdown measurements to protect the measured devices from long exposure to high reverse currents.

The other instrument is an Agilent 4284A LCR meter, which seems to be one of the most popular capacitance meters used by the semiconductor industry and different research groups. It measures capacitance according to one of two circuit models, in which the measured device is represented either by a parallel equivalent circuit or a series equivalent circuit. As per the instrument manual, the parallel model is better suited for small values of capacitance, although the distinction between small and large values is not specified. This issue will be further discussed in section 4.4.

Finally, the characterization tools would not be complete without a source of illumination. As stated above, an array of light-emitting diodes (LEDs) is used in this capacity. The LEDs come in four different colors: white, red, green, and blue. There are three diodes of each type, with total power capability of 10 W per color. The three primary colors have narrow energy distributions centered on 623 nm for the red LED, 523 nm for the green LED, and 460 nm for the blue LED. Notably, the blue diodes have a three- to four-times lower photon flux, which makes generating currents equal to J_{sc} under STC conditions impossible for most CIGS samples. In most cases, I set the light intensity to produce half of that value instead. The distinction between the effects of red and blue illumination is very important, since the former is not absorbed in CdS buffer layers. The white diode covers the whole visible spectrum, with two large peaks around 450 nm and 550 nm. Unfortunately, it is a very poor approximation of the solar spectrum, which makes calibration using solar-simulator- or quantum-efficiency-obtained

currents necessary. The uniformity of the illumination is also low, despite the presence of a wide-angle lens. This means that the measured devices need to be put close to the center of the sample stage. Nevertheless, LEDs have some important advantages over halogen lamps and more advanced solar simulators. The lack of infrared radiation significantly reduces sample surface heating, and the switching times are in the order of tens of nanoseconds, allowing for use of very short light impulses. The latter feature can be useful in measurements in the time domain, such as monitoring of the evolution or the relaxation of different processes.

4.2 Current-Voltage (IV)

While the IV measurement is one of the simplest tools in the arsenal of electrical characterization, it is doubtlessly the most useful one for solar cells, since it provides information about device performance in the most direct form. As shown in in section 2.3.4, measuring IV under illumination gives the values of short-circuit current, open-circuit voltage, fill factor, and efficiency. Additionally, a simple estimation of the series resistance and the parallel resistance can be done by extracting the slope of the light IV curve at the points where $J = 0$ and $V = 0$, respectively. Its usefulness does not end there, however, as more meaningful information can be gained from both light and dark IV curves. An example dark IV characteristic for a CIGS device measured at 200K is presented in *Figure 4.1*.

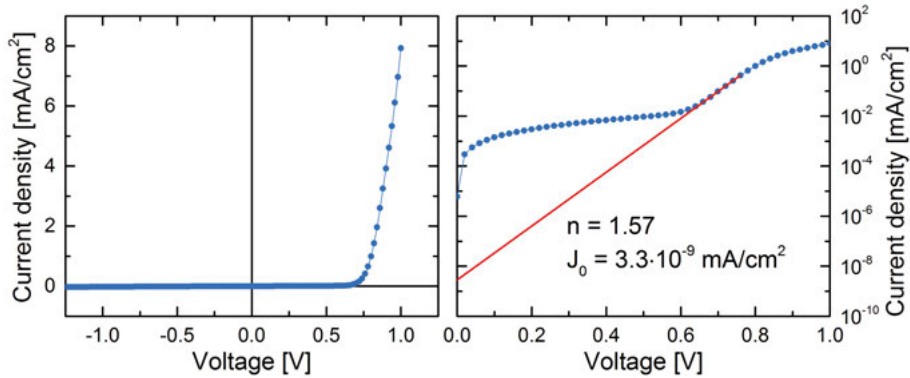


Figure 4.1. Dark IV characteristic of a CIGS device in linear scale (left) and in logarithmic scale (right), with the latter allowing extraction of the ideality factor and the reverse saturation current by fitting a linear regression line to the middle part of the curve.

A common approach to IV analysis is to plot data in logarithmic scale, as also shown in *Figure 4.1*. This allows the extraction of J_0 and n from the middle part of the curve based on equation (2.8). If this section of the curve

shows well-defined linear behavior, preferably spanning at least two orders of magnitude, it can be fitted with a linear regression line. The intercept with the current axis gives the value of J_0 , while the slope is related to the ideality factor in the following fashion.

$$\text{slope} = \frac{d(\log J)}{dV} = \frac{q}{2.3nkT} \quad (4.1)$$

For light IV data, short-circuit current needs to be subtracted beforehand. As long as the data does not deviate from linear behavior, the influence of series resistance is negligible and the corresponding term in equation (2.8) can be ignored.

A more advanced approach to IV analysis was proposed in [68] and further discussed in [18]. First, for an ohmic shunt, a plot of dJ/dV versus voltage around 0V and for reverse bias will be flat, with the level of the constant part of the curve equal to $1/R_p$. Although often some noise is present in the data, especially for illuminated IV characteristics, this method provides a better estimation of R_p than a simple extraction of slope at $V = 0$. Secondly, if $R_s/R_p \ll 1$, a plot of dV/dJ versus $(J + J_{sc})^{-1}$ should be linear for well-behaved samples, and the value of R_s can be extracted from the intercept with the dV/dJ axis, with the slope of the resulting curve equal to q/nkT . Finally, with the values of R_p and R_s known, the parasitic resistances can be compensated for in a logarithmic plot of $J + J_{sc} - V/R_p$ versus $V - JR_s$. The same methodology as in the simpler approach can be applied now, with a linear fit to the middle part of the curve giving the values of J_0 and n . This process is illustrated in *Figure 4.2* for the device from *Figure 4.1*. Note the difference in the values of extracted parameters, which shows the advantage of the more advanced approach.

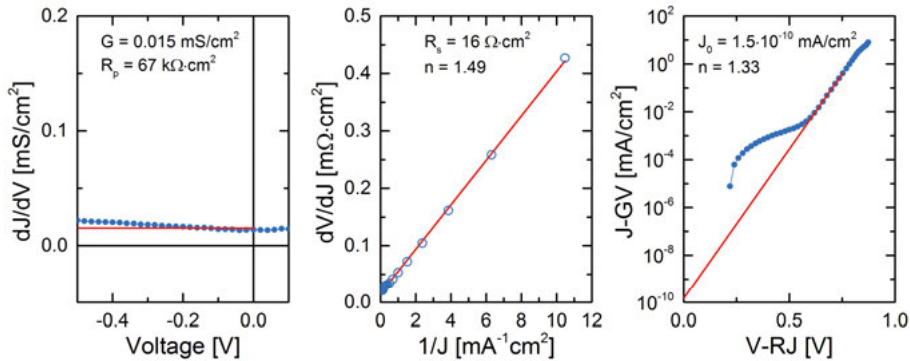


Figure 4.2. Extraction of parallel resistance (left) and series resistance (center) allows plotting of IV data with most of their contribution eliminated, which should provide a better basis for the estimation of diode parameters.

Measurement Quality

The methods of extracting information from IV data described above give good results only for well-behaved samples. In many cases, especially when dealing with metastable phenomena in CIGS devices, more advanced models are required. In some scenarios, however, the complexity of the observed behavior renders most of the discussed parameters meaningless, as the underlying physics start to deviate too much from textbook understanding of p - n junctions. While that limits *quantitative* analysis of data, *qualitative* analysis can still give meaningful results. An example of that is the analysis of deformations in current-voltage and capacitance-voltage characteristics of various CIGS devices in **Paper III**.

Breakdown Measurements

As described in section 2.2.4, when a sufficiently high reverse bias is applied to a p - n junction, it may suffer from breakdown and start to conduct a large reverse current. Thus, the IV measurement is perfectly suited for breakdown characterization. While IV characteristics are usually measured in the *forward* direction, i.e. from negative to positive voltages, it makes more sense to measure breakdown behavior in the *reverse* direction. This approach means that the reverse field in the junction increases gradually, and that the measured device can enter the breakdown more gently than if the voltage was changed in a non-continuous manner. Additionally, since any type of breakdown might cause irreversible damage to a measured device, it is usually desirable to make the IV sweep as fast as possible. On the other hand, some breakdowns are relatively slow processes, so it should be kept in mind that measurement results might be affected by the sweep rate.

One quantity of interest associated with breakdown curves is the breakdown voltage, which usually marks the point at which macroscopic reverse current starts to flow through the characterized device. However, there are two issues with this concept. First, some breakdown curves can be very gradual in nature, which makes it difficult to determine breakdown voltage. Secondly, the changes in conduction mechanisms which lead to breakdown usually occur on microscopic scale, and cannot be easily observed in a macroscopic view. Thus, for **Paper IV** I developed a method of extracting transition voltage V_{tr} , which marks the change in transport properties responsible for breakdown. The method relies on plotting the derivate of the breakdown current, and using linear regression lines to determine V_{tr} , as illustrated in *Figure 4.3*.

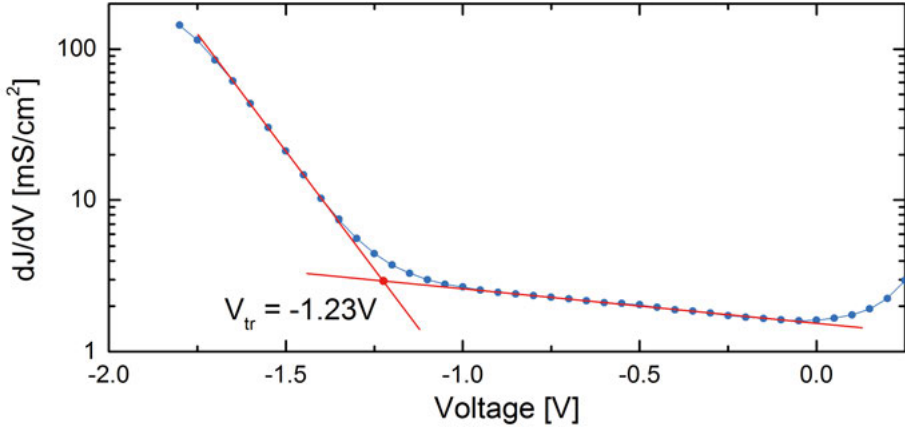


Figure 4.3. Transition voltage represents the point at which a change occurs in the main conduction mechanism in the reverse direction. Its value can be extracted from the crossing point of two linear regression lines fitted to linear regions visible in the derivative of reverse current.

4.3 Temperature-Dependent Current-Voltage (IVT)

Although temperature-dependent IV characterization relies simply on measuring multiple IV curves at different temperatures, it merits treatment as a separate measurement technique. All usual parameters can be extracted from the individual measurements and plotted as a function of temperature. Of special interest are illuminated IV curves and the thermal evolution of open-circuit voltage. First, the reverse saturation current can be expanded to:

$$J_0 = J_{00} \exp\left(-\frac{E_a}{nkT}\right) \quad (4.2)$$

The prefactor J_{00} , activation energy E_a , and ideality factor n depend on the dominant recombination mechanism contributing to J_0 . With no current flowing through the measured device at open-circuit conditions, equation (2.8) can now be rewritten as follows.

$$V_{oc} = \frac{E_a}{q} - \frac{nkT}{q} \ln\left(\frac{J_{00}}{J_L}\right) \quad (4.3)$$

Thus, a plot of V_{oc} versus temperature gives the activation energy of the dominant recombination mechanism, as illustrated in Figure 4.4. Combined with the value of the ideality factor, it can provide information about the main recombination mechanism. Unfortunately, detailed interpretation is not trivial, as it depends on the presence of Fermi-level pinning at the interface [19], [20]. At the very least, the value of activation energy points towards interface recombination when lower than the band gap of the measured de-

vice. Such information can be very useful during investigations of interface properties, as shown in some of the studies I contributed to with IVT characterization [62], [69], [70].

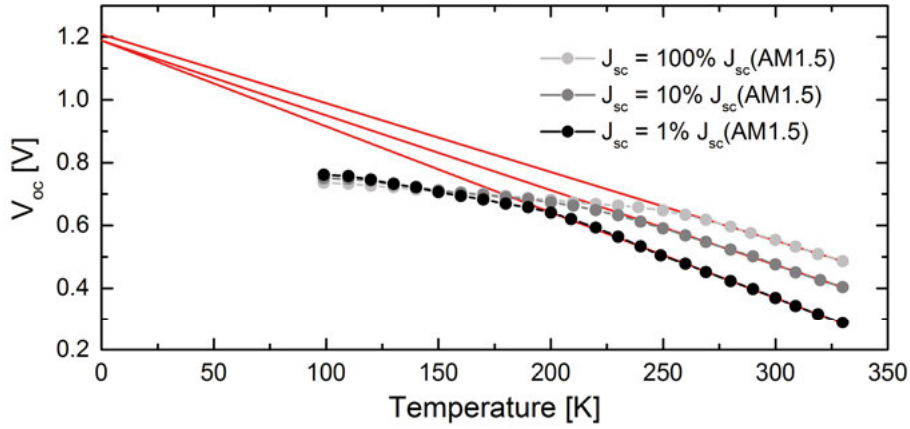


Figure 4.4. Open-circuit voltage versus temperature at different light intensities and corresponding linear fits. The point at which the fitted lines intercept the V_{oc} axis gives the activation energy of the dominant recombination mechanism.

Breakdown Measurements

Temperature-dependent IV measurements have also other uses. In **Paper I**, they were vital in the discussion about the nature of breakdowns in CIGS solar cells. Measuring breakdown curves at different temperatures revealed the temperature coefficient of the breakdown process to be negative, contrary to what could be expected from an avalanche breakdown. On the other hand, the temperature dependence was too strong to be explained by a simple tunneling process. Thus, the results of IVT characterization suggested that it was in fact a *defect-assisted* tunneling breakdown.

4.4 Capacitance-Voltage (CV)

Theory

Capacitance-voltage is a technique used to investigate carrier densities in Schottky diodes, p - n junctions, and other semiconductor devices. It relies on the fact that the width of the depleted layer changes with applied dc voltage. The magnitude of the change depends on the doping at the edge of the space-charge region, and for one-sided abrupt p - n junctions it can be assumed that only the lowly-doped side is affected. On a microscopic level, this change is reflected in the differential capacitance of the device, defined as its ability to store electric charge in response to a small change of voltage:

$$C = \frac{dQ}{dV} \quad (4.4)$$

When a junction with an area A is considered as a parallel-plate capacitor, with the distance between the plates W corresponding to the width of the space-charge region, its capacitance can be also expressed as:

$$C = \frac{\epsilon_0 \epsilon_r A}{W} \quad (4.5)$$

Thus, the value of differential capacitance can be measured with a small ac signal at different depths in the device, determined by the dc bias. Furthermore, it can be shown [67], [71] that the acceptor concentration on the p -side of a p - n^+ junction can be expressed by the following formula.

$$N_A(W) = -\frac{2}{q\epsilon_0\epsilon_r A^2} \left[\frac{d(1/C^2)}{dV} \right]^{-1} \quad (4.6)$$

Consequently, the slope of $1/C^2$ versus V , known as the Mott-Schottky plot, can provide information about the distribution of shallow doping on the lightly-doped side of the junction. An example of raw CV data, together with the corresponding Mott-Schottky plot and the derived doping profile for a typical CIGS solar cell is shown in *Figure 4.5*.

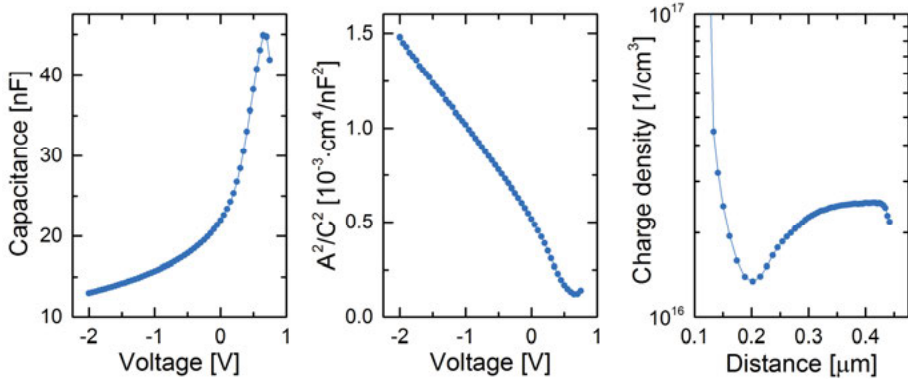


Figure 4.5. (Left) Raw capacitance-voltage data of a typical CIGS device measured at 200K. (Center) Corresponding Mott-Schottky plot. (Right) Calculated doping profile.

Practical Limitations

The presented theory of CV characterization relies on assumptions and simplifications that cannot always be realized in practice. A fundamental issue with the “doping” profiles calculated from Mott-Schottky plots is that they do not necessarily show actual doping. Since the capacitance meter measures the *current* generated by the ac voltage, and *calculates* the capacitance based

on equation (4.4) and the chosen equivalent circuit, the result is determined not only by doping but also by the response from majority carriers. In an ideal case, these two parameters would be equal, but high defect concentrations present in some devices can significantly impact the latter. Thus, a safer term to use is *charge density* profiles rather than *doping* profiles.

Defects can not only introduce errors in the analysis of charge profiles, but also distort the data in unexpected ways. Kimerling showed [72] that some combinations of doping and defect distributions can simply shift charge profiles, while others can introduce additional features, such as valleys or peaks, which are only measurement artifacts. This makes the analysis of CV data difficult in devices with large populations of many different electronically-active defects, such as CIGS solar cells. The impact of defects can be partially reduced by the choice of high ac frequency, as many deep defects cannot react to very fast changes of bias. In many cases, however, the speed of the dc voltage sweep will still be a limiting factor, as shown in [72].

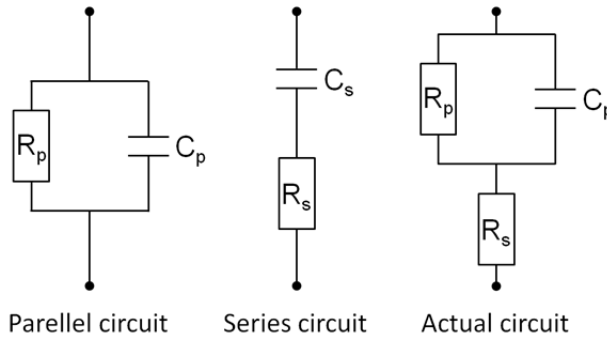


Figure 4.6. Parallel and series equivalent circuits used by CV meters and the actual circuit for most junction-based semiconductor devices.

Another issue is related to the capacitance meter itself. As mentioned above, capacitance meters assume either a parallel or a series equivalent circuit for the measured device, as illustrated in Figure 4.6. In reality, most devices feature both a parallel conductance, $G = 1/R_p$, and a series resistance, R_s . If the value of any of these parameters is too high, it introduces an error to the measured capacitance value [67]. The series equivalent circuit compensates for any series resistance, but overestimates the capacitance by a large margin if conductance becomes too high. The parallel equivalent circuit is vulnerable to high values of series resistance, but produces smaller errors with increasing conductance. A measure of quality of the measurement is the so-called quality factor Q . For the parallel circuit it is expressed by the following formula.

$$Q = \frac{\omega C}{G} = 2\pi f \frac{C}{G} \quad (4.7)$$

According to [67], a Q value of 5 or more gives a good approximation of the true value of capacitance. Since f is the frequency of the ac signal, using higher frequencies often improves the quality factor. There is a trade-off, however, as at some point carrier mobility becomes a limiting factor. For CIGS solar cells, best results can be obtained for frequencies between 100 kHz and 1 MHz. The quality factor can also be represented in the form of a phase angle between the real and the imaginary parts of impedance or admittance. The relationship between the quality factor and the phase angle is given by $Q = \tan \alpha$, so the Q value of 5 or more becomes a phase angle equal to or higher than 78.7° .

Equation (4.7) shows that high conductance reduces the quality of the measurement. This introduces additional errors when measurement conditions increase sample conductivity, and imposes a limitation on the viable measurement range. The reliability of the measurement is significantly reduced in forward bias, when the junction starts to conduct forward current, and for values of reverse bias that lead to junction breakdown. Additionally, since many semiconductor materials exhibit photoconductivity, measuring under illumination can also negatively affect measurement quality.

One more issue that requires caution is flattening-out in Mott-Schottky plots. In general, a lower slope of the $1/C^2$ curve is associated with an increase of doping. In some cases, however, the geometry of the device or the defect distribution might prevent the depletion layer to shrink or expand beyond a certain point. The corresponding charge profiles show an asymptotic increase in background static charge of many orders of magnitude. In such cases, this feature does not reflect the true charge distribution and is simply a measurement artifact.

CIGS-Specific Issues and Comments

While all previously discussed issues apply to CV characterization of many different types of solar cells, they are just the tip of the iceberg that is the measurement of CIGS devices. The main reason for that are the complex defect physics of CIGS layers [7], [73]. Two notorious specimen are the $(V_{Se} - V_{Cu})$ and the $(In_{Cu} - 2V_{Cu})$ defect complexes. The former are amphoteric defects that can act *both* as shallow donors and shallow acceptors [10], while the latter are very efficient recombination centers that *lower* their energy when capturing electrons [11], giving them shallow *and* deep character at the same time. These unusual properties are possible due to lattice relaxation around the defect sites which accompanies capture of electrons.

Although the exact details of defect properties are still a subject of discussion [74], [75], there is no doubt that their impact on electrical behavior of CIGS devices is no less than dramatic, since it manifests itself in the form of many different metastable phenomena. Examples include light- and reverse-bias-soaking [76]–[79], wavelength-dependent behavior [14], [80], and light-on-bias phenomena [23], [**Paper III**]. All these effects increase the

magnitude of the issues outlined by Kimerling [72]. At room temperature, even the direction of the CV sweep matters, as illustrated in *Figure 4.7*, because of charging and discharging of defects [81]. The same figure also shows the dependence of capacitance, phase angle, and quality factor on measurement frequency.

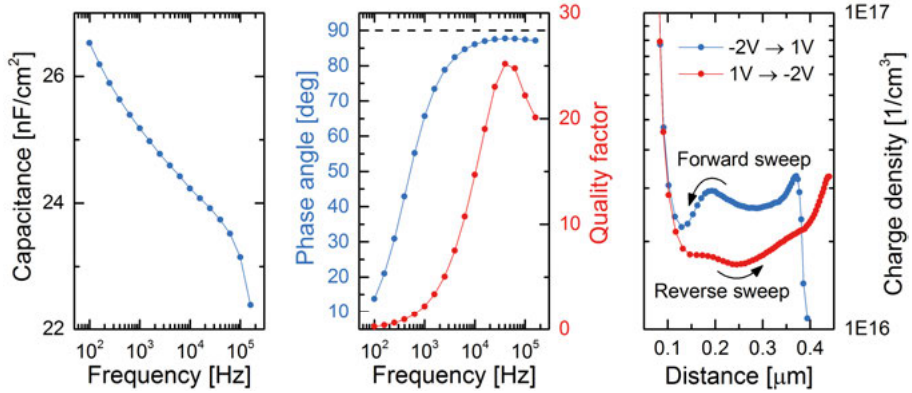


Figure 4.7. (Left) Capacitance of a typical CIGS device as a function of AC frequency measured at 300K. (Center) Phase angle and the corresponding quality factor for the same device. (Right) Hysteresis observed in charge profiles calculated from CV data measured at 300K.

Some of these issues are alleviated by measuring at temperatures below 240K [81], which freezes part of the metastable defects into configurations established at room temperature. However, even at cryogenic temperatures as low as 100K, a small degree of light-soaking is still possible. At the same time, relaxation times are many orders of magnitude higher than at 300K, which means that low-temperature measurements involving illumination necessitate a short light-soaking period to stabilize the metastable defects. This approach was used in **Paper III**, in which measurements were performed at 200K, either in the relaxed or in the light-soaked state. While it makes no difference for the latter, it could be argued that the former is no longer a relaxed state. The alternative, though, is that each consecutive measurement performed under illumination affects the state of the sample little-by-little.

The analysis of breakdown behavior in **Paper IV** revealed another possible issue with CV measurements. In that work, we presented arguments for an assumption that all reverse bias applied in darkness dropped on the buffer layer. A caveat was added, stating that the actual voltage distribution might be split between the buffer and the absorber, for example in an 80/20 ratio. If our reasoning behind the assumption is sound, it presents all manner of questions about CV characterization, the chief one being: is the actual voltage drop on the CIGS side of the junction several times lower than what we believe? This would mean that all obtained values of the width of the depletion

region in CIGS are off by up to half an order of magnitude. Despite the huge body of research on CIGS from the past 35 years, I sometimes wonder if there is anyone that truly knows these things.

4.5 Quantum Efficiency (QE)

External quantum efficiency, often referred to as simply quantum efficiency, measures the number of electron-hole pairs contributing to the photocurrent per photon of incident light. In practical terms, the characterized device is illuminated with a focused beam of monochromatic light of a given wavelength and the generated current is measured. Before the beam reaches the device, it encounters a partially translucent mirror which transmits a fraction of the beam to a monitoring detector. Since the optical properties of the mirror and of the reference device are calibrated before each measurement session, the exact number of photons in the beam can be calculated and compared with the current generated by the measured device. With the help of multiple filters and monochromators, a wide range of wavelengths, relevant to solar cell operation, can be covered. The resulting profile of quantum efficiency versus wavelength can be used to calculate the short-circuit current of the measured device under AM1.5 conditions:

$$J_{sc} = \int F_{AM1.5}(\lambda)QE(\lambda)d\lambda \quad (4.8)$$

$F_{AM1.5}(\lambda)$ is the spectral irradiance of the AM1.5 spectrum, measured in $\text{Wm}^{-2}\text{nm}^{-1}$. The resulting value of short-circuit current is usually more accurate than those measured using solar simulators, especially those not equipped with top-of-the-line light sources, since even the best simulators produce spectra different than AM1.5. It should be noted, however, that QE systems use very low illumination intensities, which can be a source of mistakes in the interpretation of results for devices with intensity-dependent transport properties. For that reason, some setups include the option of adding light bias to the measurement. To prevent the additional photons from contributing to the measured QE signal, the measurement beam is chopped and the signal is processed by a lock-in amplifier synchronized with the chopper.

An example QE curve is presented in *Figure 4.8*. Aside from providing a way to calculate the true short-circuit current of a given device, quantum efficiency spectra contain valuable information about optical and electrical losses in the measured devices. The decrease in QE value towards low wavelengths is caused by parasitic absorption in the front layers, while the decrease towards high wavelengths is due to band-gap-limited generation. More examples include shading lowering the QE overall, interference causing characteristic dips in the curve, and poor collection in the bulk leading to

additional decrease of QE for higher wavelengths. The last issue can be investigated further by plotting the ratio of QE measured with and without reverse bias, for example $QE(-1V)/QE(0V)$ [18]. Finally, the decrease in QE value at high wavelengths can be used to estimate the band gap of the measured sample. An example of band gap extraction based on a plot of QE^2 vs photon energy can be found next to the QE curve in Figure 4.8.

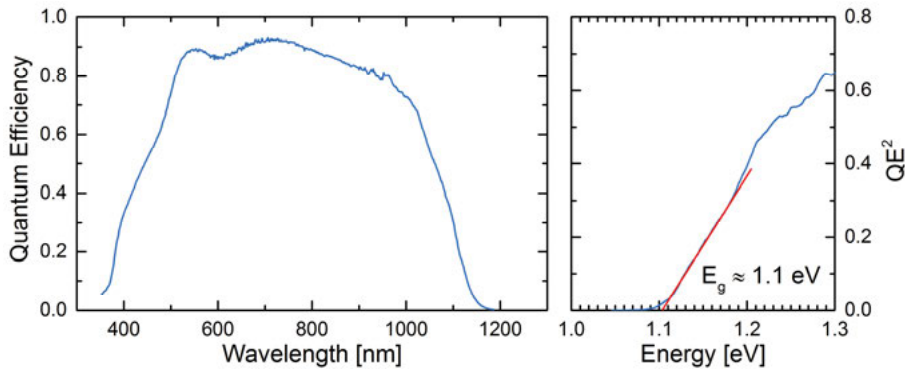


Figure 4.8. (Left) A typical QE curve of a CIGS device. (Right) Square of QE plotted as a function of energy for the high-wavelength region of the original data. Band gap of the measured sample can be estimated by fitting the low-energy part of the curve with a linear regression line.

In **Paper I**, quantum efficiency was one of the methods used to study breakdown behavior. High reverse bias was applied to the investigated samples, with its value chosen to fit between the higher breakdown voltage measured in darkness and the lower breakdown voltage measured under illumination. The wavelength sweep was then done from low to high wavelengths, which revealed that for CdS-based samples QE increased by an order of magnitude when the sweep reached wavelengths absorbed in CdS. Thus, it confirmed that absorption in the buffer was responsible for the lowering of breakdown voltage. Unfortunately, similar measurements could not be reliably performed on samples with ZTO buffers, since the current preamplifier used to strengthen the QE signal kept overloading. It would be interesting to see if the unusual QE behavior could be replicated in ZTO-based devices, despite the relatively high band gap of ZTO. As will be shown at the end of section 5.3, ZTO shows a small degree of *sub-band-gap* absorption, which can affect its electrical properties.

4.6 Measurement conditions and reproducibility

In 2011 I attended a workshop on admittance characterization of CIGS solar cells. Present were representatives of four research groups specializing in this topic. A few months before the workshop, I had prepared a number of

nearly identical CIS samples and sent them to these four groups for characterization. It turned out that very similar samples produced different results for each group, and the interpretations offered were completely different as well. There was tension in the air, and it seemed that some people were just short of calling others stupid. I doubt that any of the approaches were particularly wrong, or that these people could not properly measure the samples. Rather, they all used their own measurement methodologies and relied on their own models, resulting in an incomplete picture, pieces of which they were furiously holding onto. The simple truth is this: CIGS is a very complex material, and electrical characterization of CIGS devices is difficult and full of traps waiting for the unwary.

To reduce the likelihood of mistakes, one needs to strictly follow certain measurement rules and routines. A common pitfall is to measure something unexpected and to immediately start wondering what it could mean. Well, it does not mean anything, until one can say with a reasonable degree of certainty that the observed behavior is not a measurement artifact. With this philosophy in mind, whenever I obtain a strange result, I first ask myself: what have I done wrong? Sadly, this attitude is not as common as it should be, and many people are quick to jump to possibly erroneous conclusions³.

After eliminating the possibility that our result is a measurement artifact, the corresponding measurement should be repeated to see if the result is reproducible. Keeping the metastable defects in mind, in many cases the measurement result can be affected by the *previous* measurement. For example, when investigating the red-on-bias effect that will be described in section 5.2, one can measure IV under red illumination starting at -2V, immediately followed by a CV measurement. For the latter, the sample is neither in the red-on-bias state nor is it relaxed, since the IV measurement itself induces some red-on-bias, which is then partially removed when the measurement reaches forward voltages. Without proper caution, however, it is easy to misjudge the state of the sample during the CV measurement. Another example is demonstrated in **Paper IV**, where consecutive dark breakdown measurements on CdS-based samples are shown to increase the breakdown voltage after each measurement.

It is also a good practice to check other samples for the same behavior as soon as possible. While it might still be interesting to investigate an effect that is unique to a given sample, it is good to know if the observed behavior is a common feature or not.

To establish a common plane of comparison between different samples, their state must be carefully monitored. Since some metastable phenomena can persist for prolonged periods of time [82], [83], it is important to determine effective relaxation methods. In most cases, moderately elevated tem-

³ Not that I am always right, since I have made my share of mistakes over the years. But I do try to be safe rather than sorry.

perature accelerates the relaxation process, while high-temperature treatments usually result in irreversible changes [84], [85]. In my experience, heating a sample to 330K for one hour in darkness is sufficient to recover from most reversible metastable states, and thus it became my preferred method of relaxation, used in all of my papers.

Treatments that induce metastable phenomena also require consistent application. If treatment time is lower than the time needed to saturate a given effect, it is important to keep it the same for all samples, so that no ambiguities can arise from possible variations. The same is true for measurement temperature. Depending on the temperature range, a difference of 10K might bring meaningful changes to device behavior.

5. Defect- and Light-Related Phenomena in CIGS Solar Cells

In this chapter, I present the three phenomena that I focused on during my studies. Although they are only a subset of the different effects that can be observed in CIGS devices, none of them is truly understood yet, despite a substantial amount of research already available. The section about reverse breakdown is more personal than the others, since it is a topic to the understanding of which I contributed the most.

5.1 Light-Soaking

In general, light-soaking (LS) is a treatment that involves illuminating the investigated device for an extended period of time. By nature, it is very relevant for solar cells, since they usually spend multiple hours per day sitting in sunlight. The effects of light-soaking using white illumination (WLS) on the performance of CIGS devices were first reported in 1986 in a study by Ruberto and Rothwarf [76], which showed an improvement of open-circuit voltage, fill factor, and efficiency throughout and after the treatment. The impacts of WLS and forward-bias-soaking were further investigated in [77], where it was shown that positive effects can persist for hours, if not days, and that poor-quality samples react more strongly to the treatments. The last observation was related to the high number of defects present in these devices. The effect has been classified as persistent photoconductivity of the CIGS absorber [86].

Since that time, many other studies have been published on the topic of light-soaking, and many variations of the original treatment have been tested. Some authors reported that longer periods and multiple cycles of light-soaking *decrease* performance [87], which might be a result of sodium migration and accumulation [88]. At the same time, moderate amounts of sodium seem to be required for the benefits of shorter-term light-soaking [89], [90]. The positive effects are diminished when LS is done at short-circuit conditions [79], [91] or when using red illumination [81]. In fact, in samples with CdS buffer layers, it is the blue part of the spectrum that is responsible for improved performance [92], [93]. Absorption in CdS causes hole injection into the interface region of the CIGS layer, neutralizing

negatively-charged defects, while electrons generated in the bulk of the absorber contribute to an increase in acceptor concentration [81]. The net result is a higher background doping level, more uniformly distributed throughout the absorber. In [10], Lany and Zunger proposed that $(V_{\text{Se}} - V_{\text{Cu}})$ defect complexes could explain the changes in charge profiles. These defects can switch between shallow donor and acceptor configurations, with energy barriers separating the two, which fits quite well with experimental observations. Extensive modelling of the influence of selenium vacancies on CV charge profiles can be found in [94].

The above description mostly covers the effects of light-soaking performed at or near room temperature, which relax at an accelerated rate at elevated temperatures [93]. However, there have been some reports of treatments at 360K or more [95], [96], and in section 4.4 I mentioned that a small degree of light-soaking was possible even at very low temperatures. This suggests to me that there are in fact multiple different phenomena related to light-soaking. I would speculate that when the treatment is very long, or when the temperature is sufficiently high, it causes migration of sodium atoms, while in other cases it is related to changes in defect occupation. In the latter case, more than one defect type might be involved.

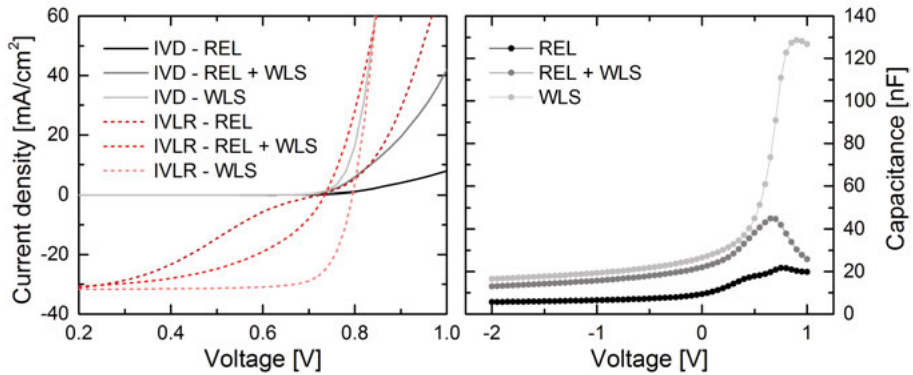


Figure 5.1. Comparison between different states of a CIGS device measured at 200K. REL stands for the relaxed state, REL + WLS for the relaxed state with 5 minutes of light-soaking after cooling down, and WLS for the light-soaked state. (Left) Dark and red IV curves. (Right) CV curves.

My chosen method of light-soaking was to illuminate the treated sample with white light of around 1-Sun intensity, for a period of 30 minutes, at room temperature. For low temperature measurements, the illumination would be kept on until the sample reached the desired temperature to prevent relaxation during the cooling period. *Figure 5.1* shows a comparison of IV and CV curves for an example CIGS device, measured at 200K in the relaxed (REL) state and after light-soaking (WLS). Additionally, the effect of 5 minutes of low-temperature light-soaking on the REL state is also shown.

Although in my work I did not focus on light-soaking in itself, I investigated its interaction with the remaining two phenomena described in this chapter. While the results were inconclusive for light-enhanced breakdown, light-soaking had a clear impact on light-on-bias behavior, as discussed in the next section and in **Paper III**.

5.2 Light-on-Bias

As the name partly implies, light-on-bias is a treatment that combines simultaneous illumination and application of reverse bias to the studied sample. Mostly known in the literature as red-on-bias (ROB), its investigation was part of my first exposure to CIGS solar cells during my Master's degree project. As shown in [23], illuminating CdS-based samples with red light, i.e. not absorbed in the CdS buffer, while applying a reverse bias of a couple of volts, results in a significant increase in capacitance due to the excess electron population causing filling of traps. In Mott-Schottky plots, a characteristic flattening of experimental curves can be observed around 0V and for positive voltages, which is associated with a massive increase of static negative charge in the CIGS layer close to the buffer/absorber interface. In many cases, the change in CV behavior is accompanied by a decrease in fill factor due to double-diode-like deformation of red IV characteristics [81], [**Paper III**]. The effect is weaker but still present at room temperature [97]. Consult *Figure 5.2* for an illustration of the described effects. The changes persist after illumination is removed, but a decrease of the bias leads to partial recovery, as the edge of the depletion region moves and holes from the bulk of the absorber can diffuse closer to the interface. Complete recovery is possible only by annealing to temperatures above 300K, or by illuminating the treated sample with a short impulse of blue light, which causes hole injection from the CdS buffer.

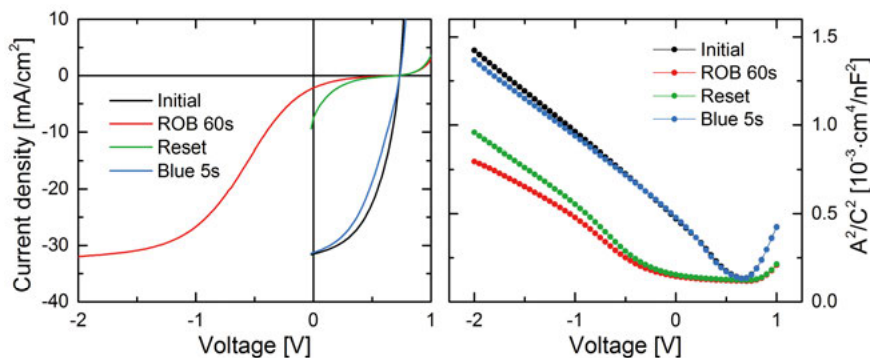


Figure 5.2. Typical red-on-bias behavior of a CdS-based sample at 200K. Red IV (left) and Mott-Schottky (right) plots show four curves each: before the treatment, after 60s of ROB at -2V, after bias reset to 0V, and after 5s of blue illumination.

The rate at which negative charge accumulates in the interface region during ROB is relatively fast, as evidenced by the fact that around 30 seconds are enough to cause an increase in static negative charge by an order of magnitude. *Figure 5.3* illustrates the evolution of charge profiles with increasing treatment time. Note that as the negative charge accumulates, it decreases the width of the space-charge region, and free holes from the neutral bulk can remove some of the charge generated at the edge of the depleted layer. In the same figure, the effect of flashing a lower voltage in-between the treatment and the measurement is also shown, partly removing the accumulated charge by allowing holes to temporarily diffuse closer to the interface. Keep in mind that otherwise the continuity of applied voltage needs to be preserved to observe the full effect of ROB, i.e. if the treatment was done at -2V the measurement sweep needs to start at the same bias, since any decrease in voltage between ROB and the measurement will affect the state of the investigated device.

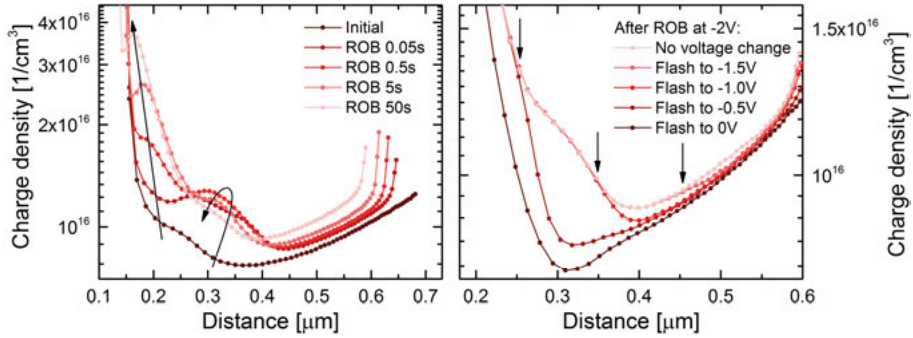


Figure 5.3. (Left) Evolution of the red-on-bias effect with treatment time. Arrows show directions of changes. (Right) Partial recovery after flashing reverse voltages lower than the one used during the treatment. Arrows mark the voltage-dependent boundary of the region accessible to free holes from the bulk.

In samples with Cd-free buffers, there is little distinction between red and blue illumination, and thus we can talk about light-on-bias in general, rather than just about ROB. Interestingly, the amount of accumulated negative charge is lower than in CdS-based samples, most of it can be removed by resetting the voltage bias, and there is little impact on IV characteristics, as shown in **Paper III**. See *Figure 5.4* for an illustration of light-on-bias behavior in a sample with a ZTO buffer layer. The difference between CdS-based samples and those with alternative buffers suggests the existence of two distinct phenomena caused by light-on-bias treatments. One can be associated with CdS buffers and the interface they create with CIGS layers, while the other with CIGS itself. Thus, the overall behavior of CdS-based samples is probably the result of a superposition of the two effects.

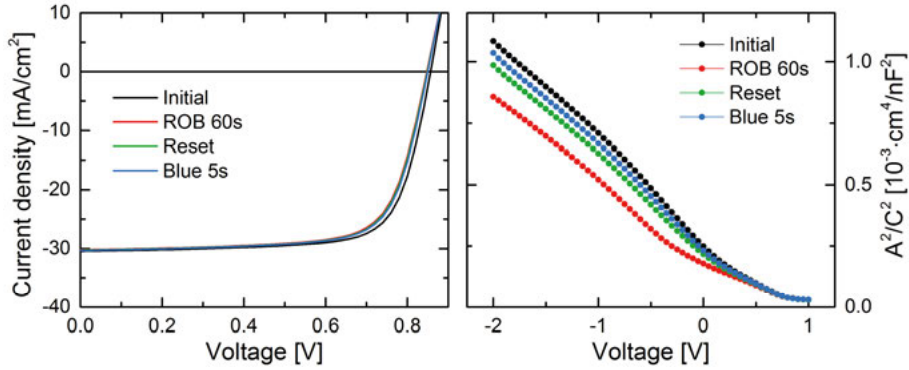


Figure 5.4. Typical red-on-bias behavior of a ZTO-based sample at 200K. IV (left) and Mott-Schottky (right) plots show four curves each: before the treatment, after 60s of ROB at -2V, after bias reset to 0V, and after 5s of blue illumination.

When investigated samples are in the light-soaked state, the degree of deformations observed in IV and CV curves significantly decreases in comparison to the relaxed state. However, **Paper III** demonstrates that the effect that light-soaking has on IV characteristics is not always consistent with the effect on CV behavior. In some samples, it all but eliminates the deformation of IV curves, while in others merely makes it milder, and both cases can be accompanied by varying degrees of decrease in CV deformation.

Theoretical Model

While the detailed physics of the general light-on-bias phenomena are not completely understood yet, one model provides an explanation for the red-on-bias effect observed in CdS-based samples. The ease with which electrons are captured in the absence of free holes and the almost instant recovery in their presence mean that the involved defects can behave as both shallow and deep traps. Such properties are associated with the $(\text{In}_{\text{Cu}} - 2\text{V}_{\text{Cu}})$ defect complexes mentioned in section 4.4. According to the extensive calculations of Lany and Zunger [11], the In_{Cu} complex acts as a substitutional shallow donor when the Fermi level is below a critical energy E_{DX} . If enough additional electrons are introduced for E_{F} to cross E_{DX} , the stable configuration of the defect changes to a deep “DX” recombination center. The transition between the two states involves capture of two electrons and lattice relaxation around the defect site. Since the red-on-bias treatment creates conditions in which the n/p ratio significantly increases in the space-charge region and close to the interface, it causes a large number of $(\text{In}_{\text{Cu}} - 2\text{V}_{\text{Cu}})$ complexes to transition to the DX configuration. Lany and Zunger postulate that together with V_{Se} -based complexes, these defects impose a limitation on the open-circuit voltage of CIGS devices [98]. Regardless of whether this model is correct or not, photoluminescence measurements clearly show that accu-

mulation of negative charge close to the interface leads to decreased current collection, resulting in the observed deformation of IV curves [22].

Impact of CIGS Composition

Since the concentrations of In_{Cu} and V_{Cu} should increase with growing copper deficiency, it could be expected that the red-on-bias effect would get stronger with a decreasing $[\text{Cu}]/[\text{Ga}+\text{In}]$ ratio. Thus, samples investigated in **Paper II** were originally meant to be used for a study of ROB behavior. Unfortunately, I did not realize at the time how much Ga gradients would be affected by the varying Cu content. While I did plenty of ROB-related measurements on those samples, in the end I could not decouple the effects of different $[\text{Cu}]/[\text{Ga}+\text{In}]$ and $[\text{Ga}]/[\text{Ga}+\text{In}]$ ratios close to the interface. Consequently, **Paper II** ended up focusing on material characterization. The next series of samples with varying Cu content used flat Ga profiles, which eliminated the most serious composition-related ambiguities. The results obtained from these newer samples, as well as from a wide variety of others, formed the basis for **Paper III**. Somewhat surprisingly, however, they showed very little correlation between red-on-bias behavior and sample composition. Thus, it seems that other factors are more important.

5.3 Light-Enhanced Reverse Breakdown

The default measurement range for IV measurements in the Solar Cell Group's characterization lab at Ångström Laboratory is -0.5V to 1.0V, but due to my experience with light-on-bias, I developed a habit of extending the range to start at -2.0V. At some point early in my PhD studies, I observed very strange IV behavior in this extended range, where the current would dip down towards higher negative values if the sample was illuminated, and then return to the regular value measured under small reverse bias. This led to further investigation, which revealed that illuminating CIGS samples with blue light drastically decreased their breakdown voltage. Some of the data from when I encountered this phenomenon, together with more typical breakdown behavior, are presented in *Figure 5.5*.

One of the first reports of this light-enhanced reverse breakdown can be found in [99], where it was shown that light absorption in the CdS buffer triggered the decrease in breakdown voltage. In the same study, the authors presented a simulation of voltage distribution in the CIGS/CdS junction at -6V without and with interface defects. In the latter case, a significant portion of the voltage dropped on the buffer rather than on the absorber. Since I could find no other publications on this topic at the time when I encountered light-enhanced breakdown myself, it was an interesting subject to explore. Unfortunately, it also proved quite frustrating, because many of the samples I measured suffered from irreversible damage due to thermal break-

downs. While some authors claim to find trends in data from randomly failing devices [100], I destroyed quite a few solar cells in the search of more reproducible results.

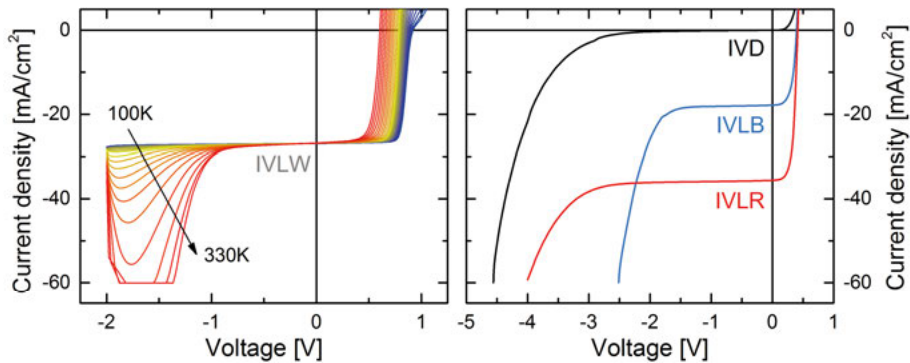


Figure 5.5. (Left) Temperature-dependent IV characteristics measured under white illumination (IVLW) in forward direction show that reverse breakdown in CIGS devices is a relatively slow process. (Right) Typical breakdown behavior in darkness (IVD), under blue illumination (IVLB), and under red illumination (IVLR). Sweeping the voltage in reverse direction allows samples to enter breakdown gradually.

One of the pressing questions about breakdowns in CIGS was whether blue illumination would also decrease breakdown voltages in samples with alternative buffers. Somewhat surprisingly, the answer turned out to be affirmative, even though blue light has lower energy than the band gaps of the tested Cd-free buffer layers. As a next step, we prepared and characterized samples with varying thicknesses of CdS and ZTO buffers. Breakdown voltages of devices measured in darkness strongly increased with growing buffer thickness, while those measured under blue illumination were consistently lower but remained mostly unaffected by buffer thickness. At the same time, temperature-dependent IV revealed that both dark and blue breakdowns had rather large negative temperature coefficients. These results were presented in **Paper I**, in which we also proposed that the breakdown mechanism was defect-assisted tunneling.

It was a few years before I returned to the topic of reverse breakdown in CIGS solar cells. As far as I know, only two papers were published on this subject during that time. Notably, one of them [101] proposed a model explaining dark and blue breakdowns with Poole-Frenkel conduction. This model was then used to fit the temperature-dependent data for CdS-based samples from **Paper I**, which I provided to the authors upon their request. On closer inspection, however, the resulting fits were somewhat unconvincing. The authors also neglected to consider the difference in voltage distribution over the CIGS/buffer junction in darkness and under illumination. Unsatisfied with their explanations and with the continued lack of other research on breakdowns in CIGS, I returned to this topic while investigating

the wide array of samples presented in **Paper III**. My hope was that measuring breakdown behavior on multiple samples with different compositions would provide more insight into this phenomenon. Even though I produced quite a lot of data, I soon realized that it was too inconclusive and that a much larger sample pool would be needed to obtain more convincing results. Part of the discarded data is presented in *Figure 5.6*. While it could be argued that some trends are visible, they are not sufficiently clear with the available number of data points, both composition- and voltage-wise.

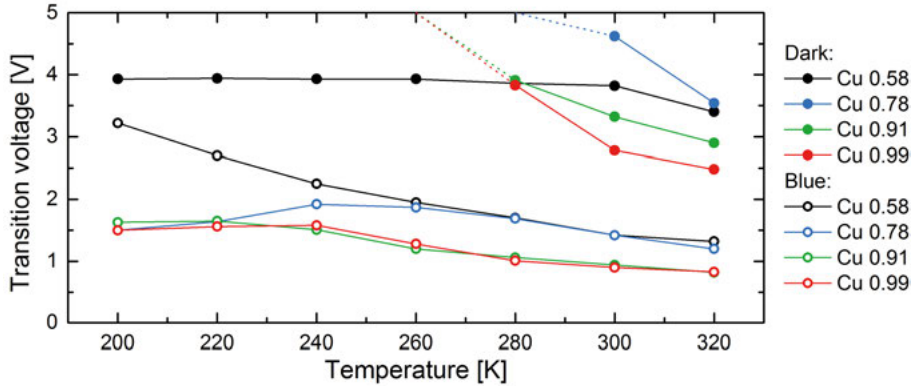


Figure 5.6. Transition voltage versus temperature for CIGS samples with different [Cu]/[Ga+In] ratios extracted from breakdown curves measured in darkness and under blue illumination. Shown values represent reverse bias. Dotted lines show that some data extended beyond the used measurement range.

Thus, together with Paweł Zabierowski from Warsaw University of Technology, a long-time collaborator with the Ångström group, we returned to the original data from **Paper I** to study it in more detail. We considered different models of the band structure of the CIGS/buffer heterojunction and different transport mechanisms, from Fowler-Nordheim tunneling (F-N), to Poole-Frenkel conduction (P-F) and electron hopping [102]. After eliminating most of them due to inconsistencies with other phenomena observed in CIGS devices, we developed a model for the dark breakdowns based on a combination of F-N and P-F conduction mechanisms, modified by series and parallel resistances. Considered in isolation, Fowler-Nordheim tunneling produces currents that increase more steeply than the measured breakdown currents. However, the fit can be significantly improved by the inclusion of series and parallel resistances. On the other hand, currents governed by Poole-Frenkel conduction are too gradual in nature, and thus cannot be adjusted in the same manner. This makes the choice of P-F conduction as the basis for the model proposed in [101] somewhat puzzling. In the end, a combination of both mechanisms gives the best results. Examples of fitted curves for CdS-based devices are shown in *Figure 5.7*. **Paper IV** includes more detailed explanations, with focus on ZTO-based samples. Regrettably, the

complexity of the phenomenon meant that we were not able to extend our model to blue breakdowns. However, **Paper IV** also mentions that the change of the breakdown voltage under blue illumination might be simply a result of photoconductivity of the buffer layers. This is a well-known property of CdS films [103], [104], which have a sufficiently low band gap to absorb some of the blue light. In contrast, ZTO layers should not be affected by blue illumination since it has lower energy than the band gap of ZTO. However, based on as of yet unpublished data, it appears that *sub-band-gap* absorption increases the conductivity of ZTO layers, which can be seen in *Figure 5.7*.

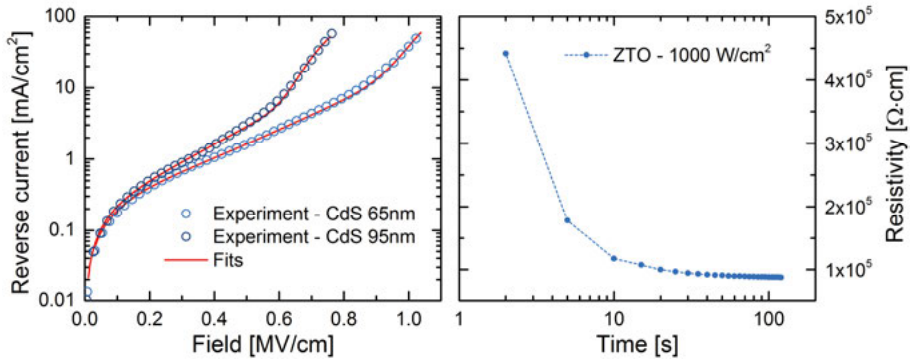


Figure 5.7. (Left) Breakdown data for two samples with different CdS buffer thickness. Red lines are fits based on the combined F-N/P-F model. (Right) Resistivity of ZTO versus illumination time.

6. Overview of Papers

In this section, I present the papers which I wrote throughout the course of my studies. While there are other articles that I contributed to in various ways, these four were mostly my own work, and thus truly represent the core of my thesis. The remaining papers are listed in the beginning of the thesis under the label Related Papers.

6.1 Paper I: Light-Enhanced Reverse Breakdown in Cu(In,Ga)Se_2 Solar Cells

Background and motivation

Reverse breakdown in CIGS was not a well-documented topic at the time, so it became the subject of my first research paper. With the group's manufacturing facilities, it was possible to produce samples which could provide new insights into breakdown properties.

Key findings

- The presence of blue illumination significantly decreases breakdown voltage in samples with CdS and ZTO buffer layers.
- Breakdown voltages measured in darkness strongly increase with growing buffer thickness.
- Breakdown voltages measured under blue illumination are mostly independent of buffer thickness.
- Both types of breakdown have high negative temperature coefficients, suggesting defect-assisted tunneling as the main breakdown mechanism.
- Quantum efficiency increases by an order of magnitude for reverse-biased samples with CdS buffers for wavelengths absorbed in CdS.

My Contribution

I did the electrical characterization, most of the analysis, and all of the writing.

6.2 Paper II: Influence of Varying Cu Content on Growth and Performance of Ga-Graded Cu(In,Ga)Se₂ Solar Cells

Background and motivation

Ga-graded absorber layers are commonly used in the best CIGS devices, and the optimal distributions of Ga and In are always a topic of interest. Cu content is a less-discussed subject, and most industrially-grown CIGS layers have a $[\text{Cu}]/[\text{Ga}+\text{In}]$ ratio of around 0.85 ± 0.05 . With our production facilities, we could manufacture and investigate the electrical performance of Ga-graded samples within a much wider window of Cu content.

Key findings

- Decreasing copper content enhances interdiffusion of In and Ga, which leads to reduced Ga gradients.
- Deposition processes need to be adjusted accordingly to obtain the desired gradients in samples with large Cu deficiency.
- In samples with compositions close to stoichiometry, Cu variation significantly influenced grain size.
- In samples with $[\text{Cu}]/[\text{Ga}+\text{In}]$ ratios of 0.65 and lower, Cu(In,Ga)₃Se₅ precipitation and reduced solar cell efficiency were observed.
- The sample with the lowest $[\text{Cu}]/[\text{Ga}+\text{In}]$ ratio of 0.5 still exhibited efficiency at the 13% level, showing that CIGS is remarkably tolerant to changes in composition.

My Contribution

I did the electrical characterization, a large part of the analysis, and almost all of the writing.

6.3 Paper III: A Systematic Study of Light-On-Bias Behavior in Cu(In,Ga)Se₂ Solar Cells With Varying Absorber Compositions

Background and motivation

While there are many studies on light-on-bias phenomena in CIGS solar cells, it is still unclear which defects are involved in them and which material properties are connected to their presence and magnitude. I attempted to investigate the latter by measuring a wide selection of samples and correlating their composition with the degree of deformations observed in IV and CV data after light-on-bias treatments.

Key findings

- There is a strong connection between deformations caused by red-on-bias treatments in IV and CV characteristics.
- Blue-on-bias leads to smaller deformations in CV characteristics and does not affect IV behavior.
- The negative impact of red-on-bias on IV is only observed in CdS-based samples. Samples with Cd-free buffers are free of IV deformations.
- IV and CV deformation factors were defined to correlate electrical behavior with sample composition.
- No clear compositional trends were found, suggesting that other factors are more important in determining red-on-bias behavior.

My Contribution

I did the electrical characterization, almost all of the analysis, and all of the writing.

6.4 Paper IV: Advancing the Understanding of Reverse Breakdown in Cu(In,Ga)Se₂ Solar Cells

Background and motivation

Reverse breakdown in CIGS solar cells continues to evade full understanding and few publications explore this topic. In the time since **Paper I** had been published, a model based on Frenkel-Poole conduction was proposed as an explanation for the observed breakdown behavior. However, the provided interpretation of experimental results was unsatisfactory, which prompted us to reexamine the data from **Paper I** and to develop our own model.

Key findings

- Transition voltage was proposed as a more meaningful alternative to breakdown voltage, along with a method to extract it from IV curves.
- The distribution of voltage over the CIGS/buffer junction was discussed.
- It was assumed that all voltage drops over the buffer layer in darkness.
- Conversely, under illumination the voltage drop shifts to the CIGS layer.
- Electric field was calculated for the dark breakdown data and different transport mechanisms were considered.
- A model combining Fowler-Nordheim tunneling and Poole-Frenkel conduction was proposed to explain dark breakdowns in CIGS devices.

My Contribution

I did the electrical characterization, implemented all of the analysis methods, and did all of the writing.

7. Concluding Remarks

Summary

With the amount of solar power reaching the surface of the Earth, photovoltaic technology has the most potential out of all renewable energy sources. And yet, most countries are still slow in adopting it as one of their primary methods of electricity generation. In many cases, it is a matter of cost, since fossil fuels tend to be cheaper than renewable energy. The “hidden” costs of burning fossil fuels, that some politicians stubbornly disregard, are increased pollution and the danger of catastrophic global warming. This is why driving down the monetary costs of photovoltaics is not only important for the profit-oriented industry, but also serves as a vital motivation for solar cell researchers.

In this thesis, I focused on electrical characterization of CIGS solar cells and on certain phenomena related to their performance in the hope that pushing the understanding of the underlying physics might bring tangible improvements to device efficiency. I have to admit that for the most part, I have only a slight idea about the subjects I explore. CIGS itself and its characterization are such complex topics that I cannot really claim to have any deep understanding of them. That said, I have tried to contribute to the field of CIGS solar cells with research that others may find useful or build upon.

Although not a particularly hot subject, reverse breakdown studied in **Paper I** and **Paper IV** can be a real issue in commercial CIGS modules. Better understanding of the phenomenon could allow module manufacturers to reduce the number of bypass diodes per module, or even eliminate them completely. I believe the two papers are a significant contribution to this subject. Both show results on samples with CdS and ZTO buffers, proving that light-enhanced breakdown is not a CdS-specific effect. As far as I know, **Paper I** is also the first study to show temperature-dependent breakdown behavior in CIGS devices. At the same time, **Paper IV** presents one of the only two published models attempting to explain the physics behind the breakdowns.

Paper II does not feature any major discoveries, but adds to the pool of knowledge about Ga gradients and the impact of Cu content in CIGS absorbers. The most interesting insight is that even layers with $[Cu]/[Ga+In]$ ratios as low as 0.5 can result in devices with decent conversion efficiencies.

To better understand the impact of CIGS composition on light-on-bias behavior, I obtained a lot of results that were meant to be presented in **Paper III**. However, the amount of data was quite overwhelming, so I employed some statistical methods to correlate the shapes of IV and CV curves with sample composition. With this approach, I was able to extract information that would have otherwise stayed hidden in the more qualitative results. Since I cannot recall any similar examples of handling electrical characterization data in the CIGS literature, I hope it also provides some food for thought for the reader.

Additional Thoughts

On a more philosophical note, over the course of my studies I wrestled with the following two questions:

- Can CIGS devices be truly understood at a fundamental level?
- If they can, is it worth the effort?

After all, even after more than 40 years of research, CIGS still holds quite a few secrets. In the meantime, silicon continues to dominate the commercial market, and newer materials, such as kesterites and perovskites, are being considered as the alternatives or successors to CIGS. While I do not feel qualified to judge how favorably CIGS compares to these other materials from the industrial point of view, I am rather positive that it is a solid solar cell material in general. From a purely academic point of view, CIGS is a very interesting compound, but one that can also be quite frustrating to study. CIGS-based devices can sometimes seem like magical black boxes with input and output terminals. We know what comes in and we know what comes out, but what happens inside is anyone's guess. Of course, this is somewhat of an exaggeration, although one that can all too quickly feel like reality when you work on some CIGS-related problem just by yourself.

With that in mind, let us now come back to the first of the two questions opening this chapter. I *do* believe that we can gain a much better understanding of CIGS devices. That said, I think it requires a fusion of different approaches, which is not necessarily easy to achieve. Material and electrical characterization, simulations, and theoretical calculations should support each other much more closely than they do right now. Most research groups specialize in one or two of these areas and focus on a limited number of phenomena, which only gives them access to a part of the larger picture. The amount of competitiveness in modern science does not help the issue, as illustrated by the anecdote which opens section 4.6. If all the bickering about whose interpretation is better could be replaced by efforts to synthesize the different approaches, it would take us a long way towards improving the status quo. I believe that better cooperation is also a remedy to sloppy science. Too many mistakes are simply a result of ignorance that could be fixed by having a dialogue with someone more experienced. Too often, though, pride or fear hamper our ability to ask for help in a field in which knowledge

is regularly equated with prestige. While it might seem that I digressed a lot from the original question, all these issues are very real obstacles to a better understanding of a material as complex as CIGS.

Thus, we come to the second question. Historically, most of the major advancements in CIGS solar cells were the result of chance or trial and error approaches. Companies such as Solar Frontier have huge manufacturing facilities, allowing them to test many different ideas in a short span of time. In many cases, trial and error can be much more efficient in finding correlations between different deposition parameters than more deliberate attempts at understanding the underlying physics. It does not mean, however, that one can put a bunch of apes in a CIGS factory in the hopes of getting increased cell efficiency over time (but if you do, record it for me). A certain amount of understanding is necessary to know in which direction to probe, but once the direction is established, it is easy to wait and see which variations give the best results. The efficacy of this process is what makes me question whether a deep understanding of CIGS is worth the significant effort it would require. Regardless of which approach is objectively better, I believe that future improvements in CIGS technology will be through smart engineering rather than understanding of interesting but perhaps ultimately obscure electrical phenomena.

Summary in Swedish

Med det överhängande hotet om klimatförändringar måste mänskligheten nu, mer än någonsin, fokusera på förnybara och miljövänliga energikällor. Trots det så går det för de flesta länder långsamt att ställa om sin energiproduktion till förnybar energi, med vissa få undantag. I många fall är det en kostnadsfråga, eftersom fossila bränslen tenderar till att vara billigare än förnybar energi. Politiker bortser ofta från den ”dolda” kostnaden med förbränning av fossila bränslen, som är ökande föroreningar och hotet om en katastrofal global uppvärmning. Efter över ett sekel med otrolig teknisk utveckling verkar vissa tro att vi äger planeten Jorden. Det är förstås långt ifrån sanningen. Med stor makt följer också stort ansvar, ett ansvar gentemot våra barn och deras barns framtid. Vi har bara planeten till låns och vi måste ta hand om den. Ett av de bästa sätten att göra det är att använda förnybara energikällor, såsom sol, vind, vatten och geotermisk energi, för att täcka vårt nuvarande och framtida energibehov. Den här avhandlingen handlar om solenergi.

Ljuset och värmen från solen är nödvändigt för livet på jorden. Utan dessa skulle jorden bara vara en naken livlös klippa i rymden. Fryst till $-273\text{ }^{\circ}\text{C}$, den absoluta nollpunkten, skulle den för evigt driva omkring i rymdens mörka, ogästvänliga vakuum. Det är häpnadsväckande att på 150 miljoner kilometers avstånd från vår stjärna så kan solens strålning värma upp jordens yta till över noll grader. Man behöver inte vara fysiker för att förstå att energimängden från solen är enorm. Faktum är att solen är den absolut största energikällan vi har tillgång till, många gånger större än alla andra tillsammans.

Medan ett sätt att tillvarata solens energi är att utnyttja dess förmåga att värma upp olika föremål, så finns det ett mer praktiskt sätt att direkt generera elektrisk energi från solens strålning. Redan 1839 upptäckte Becquerel att belysning av vissa material resulterade i en generering av en elektrisk ström. Det är detta fenomen som i princip är grunden till dagens solceller. Dryga 100 år efter Becquerels upptäckt demonstrerades de första praktiska solcellerna av Bell Laboratories i USA år 1954. De var baserade på kisel, ett av de mest vanliga naturligt förekommande materialen på jorden, och som också är det material som i huvudsak används inom modern elektronik. I början användes solceller mest i rymdtillämpningar, men så småningom så sjönk tillverkningskostnaderna så att det blev intressant för elgenerering även här på jorden.

Idag så står solceller för en kraftigt ökande andel på marknaden för elgenerering, med Kina, Japan och USA som de länder som står för hela två tredjedelar av den totala installerade solcellskapaciteten år 2015. Samma år stod solceller för 29% av andelen förnybar energi, och 1.2% av det totala globala energibehovet. Marknaden domineras fortfarande av kiselbaserade solceller, vilka år 2015 stod för mer än 90% av solcellskapaciteten. Solceller baserade på tunnfilmsmaterial ligger långt efter, med en andel motsvarande bara 6%.

Trots en ganska liten marknadsandel så har tunnfilmssolceller flera fördelar gentemot kisel, som har låg kostnad och bra prestanda att tacka för sin popularitet. Många tunnfilmsmaterial är faktiskt bättre lämpade för solceller än kisel, med både bättre elektriska och optiska egenskaper. Dessutom är materialåtgången mindre, och möjligheten att belägga de tunna filmerna på olika sätt och på olika substrat större.

Ett av de mest populära tunnfilmsmaterialen är Cu(In,Ga)Se_2 , ofta förkortat som CIGS. Rekordet för verkningsgrad för CIGS är (i labbskala) 22.6%, vilket är tre procentenheter lägre än rekordet för kisel. Det finns uppenbarligen förbättringspotential för tunnfilmsmaterial, och fokus i denna avhandling ligger därför på elektrisk karaktärisering och förståelse av, de ibland besynnerliga fenomen, som vi finner i tunnfilmssolcellerna tillverkade av CIGS.

Solceller i CIGS fungerar i princip som andra solceller. Det som vi uppfattar som ljus kan liknas vid ett flöde av partiklar som kallas fotoner, och synligt ljus är bara en del av ett större spektrum av elektromagnetisk strålning. Olika färger hos ljuset motsvarar fotoner med olika våglängder och energier. När en foton tränger in i ett halvledarmaterial, som t ex CIGS, så är det materialets energibandgap som är den avgörande egenskapen som styr sannolikheten för om fotonen kommer att absorberas i materialet eller inte. Om fotonens energi är större än bandgapet så är absorption möjlig. Tvärtom så beter sig materialet genomskinligt för fotoner med lägre energi än bandgapet. Vid absorption så avger fotonen sin energi till elektroner bundna vid atomer i materialet. De negativt laddade elektronerna, liksom tomrummet de lämnar efter sig (positiva hål), blir nu fria laddningar som kan röra sig fritt i materialet. Om en bestrålad solcell ansluts till en elektrisk krets kan man mäta en elektrisk spänning och en elektrisk ström där den maximala strömmen är proportionell mot antalet absorberade fotoner. Produkten av spänning och ström är då lika med den genererade effekten. Förhållandet mellan genererad effekt och den tillgängliga effekten i det infallande ljuset är det som kallas verkningsgraden.

En solcell av CIGS består av flera tunna lager som är belagda i en bestämd ordning. En typisk belägningsprocess kan bestå av följande steg. Först deponeras ca 500 nm Molybden (en elektrisk ledande metall) på ett glassubstrat med en metod som kallas sputtering, för att utgöra solcellens ena elektriska kontakt (bakkontakten). Därefter deponeras ca 2 μm CIGS med en metod där de fyra olika materialen förångas från separata källor, samtidigt som substratet värms till ca 500 °C. CIGS är det lager som ska

absorbera ljuset och blir vid tillverkningen naturligt p-typ, dvs det har ett överskott av fria hål som laddningsbärare. Ovanpå lagret med CIGS läggs ett bufferlager som är av n-typ, som innebär att elektronerna här är i överskott. CIGS och buffer bildar då vad som kallas en p-n övergång, vilket är en av de viktigaste strukturerna inom halvledarelektroniken. Som buffer används typiskt ca 50 nm av materialet CdS, som beläggs med en våtkemisk process. Mindre giftiga material, fritt från Cd, undersöks också. Slutligen deponeras en ca 500 nm genomskinlig ledare som framkontakt till solcellen. Här används vanligtvis ZnO med små mängder Al för att erhålla önskade elektriska och optiska egenskaper.

Att CIGS naturligt är p-typ beror på den komplexa defektfysik som materialet uppvisar. Till skillnad mot flera liknande material är energiåtgången för att bilda defekter i CIGS väldigt låg, i vissa fall t o m negativ. Detta leder till en extremt hög koncentration av defekter. Både p- och n-typ defekter finns i hög koncentration i CIGS men kompenserar varandra till stor del, så att den resulterande nettodopningen blir p-typ i en koncentration flera tiopotenser lägre än den faktiska koncentrationen defekter. Detta leder i sin tur till att flera ovanliga elektriska fenomen kan observeras i CIGS. Tre av dessa studeras i avhandlingen: light-soaking (ljusbehandling), light-on-bias (ljusbehandling med pålagd spänning), samt light-enhanced reverse breakdown (elektrisk genombrott beroende av ljus).

Light-soaking är en behandling där solcellen som ska undersökas utsätts för ljus under en längre tidsperiod. Eftersom solceller vanligtvis utsätts för flera timmars solljus per dag, så är det här naturligtvis relevant för dess funktion. För de flesta solceller i CIGS så förbättras flera parametrar som är relevanta för solcellen som t ex verkningsgraden, fyllnadsfaktorn och spänningen under och efter ljusbehandlingen. Förbättringarna kvarstår efter flera timmar och ibland dagar, och solceller av sämre kvalitet svarar ofta kraftigare på behandlingen, vilket förklaras av att effekten är relaterad till antalet defekter i materialet. Samspelet mellan ljusbehandling och de två andra fenomenen undersöktes som en del i avhandlingen. Resultaten visade att ljusbehandlingen har en stor påverkan på light-on-bias, men liten eller ingen påverkan på light-enhanced breakdown.

Light-on-bias är en behandling som kombinerar effekten av belysning samtidigt som en negativ spänning läggs över solcellen (reversed biased). Av speciellt intresse är red-on-bias, alltså belysning med bara rött ljus, vilket inte absorberas i CdS bufferlagret. En sådan behandling skapar ett överskott av elektroner vilka kan fylla upp fällor/tillstånd i CIGS-lagret, och på så vis kraftigt öka den uppmätta kapacitansen över solcellen. Fångade elektroner kommer uppfattas som statisk negativ laddning och speciellt området kring gränsskiktet mellan CIGS och CdS är känsligt för infångade elektroner, och därmed påverkan av kapacitansen. I många fall leder ökningen i kapacitans till att solcellens prestanda försämras vid belysning med rött ljus. Om belysningen upphör, men den pålagda spänningen kvarstår, så består effekten av

red-on-bias. Men minskas nu spänningen så återhämtar sig materialet delvis, dvs den statiska negativa laddningen minskar. Fullständig återhämtning är möjlig om solcellen bestrålas med mer energirikt blått ljus, vilket delvis absorberas i bufferlagret och orsakar injektion av hål (positiv laddning) från Cds till CIGS. För solceller med alternativa bufferlager (alltså utan Cd) så är det liten skillnad mellan röd och blå belysning, och den resulterande ökningen i kapacitans blir mindre. Samtidigt, så ändras inte heller solcellens prestanda nämnvärt.

Elektriskt genombrott kan uppstå om tillräckligt hög negativ spänning läggs över en p-n övergång, vilken normalt sett blockerar strömmen i den riktningen. Går komponenten i genombrott, dvs den pålagda spänningen överstiger den s k genombrottsspänningen, så kommer en stor ström att flyta vilket kan leda till permanent skada av solcellen, främst beroende på den lokalt kraftiga temperaturökningen. Resultaten visar att genombrottsspänningen för en CIGS solcell minskar vid blå belysning. Bakomliggande orsak till detta finns det fortfarande inte någon tillfredställande förklaring till, och därmed ingen exakt fysikalisk modell. Däremot så föreslås i avhandlingen en modell som förklarar genombrotten i solcellerna utan belysning. Modellen förutsätter att den pålagda spänningen i huvudsak ligger över bufferlagret i mörker och över CIGS-lagret vid blå belysning. Det höga elektriska fältet i bufferskiktet möjliggör Poole-Frenkel-transport och att Fowler-Nordheim-tunnling är den dominerande ledningsmekanismen mellan bufferskikt och CIGS-skikt. Vid blå belysning ändras beteendet, vilket troligtvis är beroende på att bufferlagrena uppvisar fotokonduktivitet, dvs att ledningsförmågan ökar med belysning.

Acknowledgements

At last we come to the acknowledgements. I cannot really express all the gratitude that I feel towards the people that I encountered throughout my studies, but I will try to put at least some of it into words. Academia can be a sad place for building relationships with people that one works with, since many leave before one had a chance to realize how good of a friend they had become. I apologize to all those who feel like they should have gotten some more space here and to those who I should have mentioned but failed to. My memory can be fickle when I try to probe such a vast part of it.

- **Marika**, thank you for inviting me into the group and for believing in me throughout the course of my studies. You certainly had reasons to worry about my progress, but your seemingly endless reservoirs of positive energy have always been inspiring.
- **Uwe**, you are special. Your commitment to students and teaching is beyond exemplary. I have always felt that I could talk with you on any topic and always learn something new. You are also a most pleasant companion and a good friend. Okay, enough, I am sold. I will take two of you.
- **Jörgen**, to think I used to be a little scared of you in the beginning brings a smile to my face now. You have turned out to be the second most reasonable person in the division, right after me. Your support at the end of my studies was invaluable. The amount of genuine interest you have shown in my research still continues to amaze me. I nominate you for prime minister of Sweden.
- **Shili** and **Zhen**, thank you for the outsiders' perspective on my thesis.
- **Lotten** and **Tobias**, thank you for the few times we had a chance to work together on something. Observing you at work has definitely contributed to my growth as a researcher.
- **Adam**, I really missed you when you left for the US. You cannot imagine how much it lifted my spirits when I learned that you were coming back. PogChamp. You are a dear friend and a brother in cynicism. For our own good, though, we need to limit the Kappa a bit, I think... I hope you will eventually end up in a place you will feel happy about <3
- **Viktor**, you were the best roommate I could wish for. We did not always agree on every topic, but there was nothing we could not discuss. The mutual understanding we shared about our little room made it into an oasis in the midst of what sometimes seemed like a scorching desert.

Thank you for these years of companionship. I put your photo on the wall and gave you the mustache you deserved.

- **Pedro**, I have a suspicion your laughter attracts unicorns and other creatures of myth. It should be recorded and sent out with the next Voyager probe as the ultimate message of peace. On second thought, such a recording could be dangerous when looped. Who could ever stop rolling on the floor with laughter upon hearing such endless mirth? You were the first to grace the wall of my office with a photo of your face, and the first to be granted the honor of mustache.
- **Bart**, there is no gentle way of putting it. You are a pervert. I can only imagine all these people that think you are a perfectly nice, even-tempered guy, but I know the darker truth. Still, that was one of the reasons it was never dull hanging out with you. Do I even need to mention the mustache at this point?
- **Christopher**, I had never met a real hipster before making your acquaintance. Keep the sausage rolling and look out for those drafts indoors. You need to protect your ears a bit more, wearing a hat just on the tip of your head will not do. Sometimes you seem crazy, but I love your company anyways (as long as I am outside the blast radius when you eat something with your hands). Also, there is scarcely better entertainment than listening to you trying to explain the plot of a movie.
- **Kirderf**, you ugly bastard. Working with you could be as infuriating as hanging out with you could be fun. You were one of my most reliable lunch buddies all the way until you were not. Whenever I think about you, I feel conflicting urges to punch and hug you at the same time. What else is it if not love? Also, for the Emperor!
- **Larsk**, sometimes I feel bad about all the fun I poke at you, but then I remind myself that you know that I know that you know that it is all just harmless and that I actually like you. You will not hear that from me ever again, but I even respect you. There, do not smile too widely and never mention it to anyone. Go on, bugger off.
- **Balazs**, you were bonkers, but I felt a connection with you, and I was really sorry to see you leave. It seems like you made a right decision, though, so I am happy for you. Your feats of ingestion became the stuff of legends, forever immortalizing you in our little lunch circle as the Hungarian. But I will also remember you fondly for all the occasions we played board games or did other things together.
- **Jan**, you are a funny guy, and sometimes it is even intentional. I am sad whenever you have a lunchbox, because that means you will not keep me company during lunch. When you do participate, though, there is always something to talk about.
- **Timo**, for a long time we were the two grumpiest guys in the group and that made me feel a special connection with you. I always liked how you identified yourself as either German or Belgian, depending on what was

more convenient on a given occasion. Also, for the last time, there were more pieces of cake than people at that party and I was not covering the second piece with whipped cream.

- **Sebastian**, I miss your quirky and insightful comments about all kinds of things, with linguistics in particular. Somehow, you always had a Monty Python quote ready for every occasion. It was also interesting to learn about your unusual musical hobby. Who knew such weird instruments existed.
- **Jonas**, you were a guy who could appreciate a good lame joke (it is not an oxymoron to people in the know). I think you would enjoy the one I came up with about Germans crowding a place, but maybe it is better left unwritten.
- **Johan**, what a strange person you are. We started our studies within two weeks of each other, but I do not think I ever really understood what made you tick. You are a true gentleman, though, and you have always impressed me with your composure and professional approach to your duties. I hope you have overcome the issues we both struggled with.
- **Milena**, you are such an amazing person. There is little I can say that will do you justice. Your kindness, warmth and positive attitude have always made your company a blessing. Thank you for all the sweets you shared with me throughout the years.
- **Shuyi**, you are my favorite Chinese person ever. Oh wait, that might not be a politically correct thing to say. Another attempt: Shuyi, you are ranked somewhere among my favorite people, maybe around rank 42. Sounds much better, right? I wish you did not have to leave our group. That was a sad day for me.
- **Dorothea**, I just want to commend you for the progress you have made since starting in our group. I am sorry to see that some of your dreams and idealistic notions seem to have been crushed in the process, but you have definitely evolved as a person.
- Thank you to other members of the solar cell group and of the division that I interacted with in one way or another: **Per-Oskar**, **Tove**, **Tomas K**, **Jonathan**, **Sara**, **Shabnam**, **Jens**, **Whitebrow**, **Ray**, **Olivier**, **Carl**, **Jes**, **Katharina**, **Sven**, **Fredrik L**, **Patrik**, **Malkolm**, **Lukas**, **Nina**, **Vododymyr**.
- **Pawel**, thank you for all the fruitful discussions we have had throughout the years. Your knowledge and understanding of CIGS are far beyond mine. I am sorry I got so angry at you when our communication stopped for some time. You can be disorganized and always bite more than you can chew, but you have never showed anything other than goodwill towards me.
- **Uwe** and **Daniel** from Solibro, thank you for your almost constant presence throughout the years. It was always nice to chat with you guys, and

I always respected your work, especially since you really helped to keep all the equipment running. It would not be the same without you guys.

- **Herman and Wolfgang**, it was a pleasure making your acquaintance and hearing some of your stories. Your presence in the division was inspiring. I was very sad when Herman passed away, but I know there are people who will cherish their memories of him.
- **Marianne, Olof, Ramy**, thank you for administering the division. Without your efforts everything would fall apart. Special thanks go to Marianne, who helped me on countless occasions during the first years of my studies.
- Finally, a big thank you to my wonderful wife **Marta** and my amazing daughter **Klara**, I love you with all my heart. Your patience and continued support were invaluable. I might not always act like it, but without you I would be even more lost in life. My dear **parents** and **grandparents**, thank you for your unwavering belief in me. Sometimes I was frustrated that you could not truly understand some of my problems, but I could always count on your unconditional love. I also thank the rest of my **family** and **friends** back in Poland. Even if we do not meet very often, I remember about you and cherish our shared memories.

I would like to thank the StandUp for Energy initiative for providing the funds for my studies.

Bibliography

- [1] “IEA PVPS Trends in Photovoltaic Applications - 21st Edition - 2016,” 2016.
- [2] P. Jackson, R. Wuerz, D. Hariskos, E. Lotter, W. Witte, and M. Powalla, “Effects of heavy alkali elements in Cu(In,Ga)Se₂ solar cells with efficiencies up to 22.6%,” *Phys. Status Solidi RRL – Rapid Res. Lett.*, vol. 10, no. 8, pp. 583–586, Aug. 2016.
- [3] M. A. Green *et al.*, “Solar cell efficiency tables (version 49),” *Prog. Photovolt. Res. Appl.*, vol. 25, no. 1, pp. 3–13, Jan. 2017.
- [4] M. A. Green, *Solar Cells : Operating Principles, Technology and System Applications*. Kensington, N.S.W.: University of New South Wales, 1998.
- [5] M. I. Alonso, M. Garriga, C. A. D. Rincón, E. Hernández, and M. León, “Optical functions of chalcopyrite CuGa_xIn_{1-x}Se₂ alloys,” *Appl. Phys. A*, vol. 74, no. 5, pp. 659–664, May 2002.
- [6] T. Dullweber *et al.*, “Back surface band gap gradings in Cu(In,Ga)Se₂ solar cells,” *Thin Solid Films*, vol. 387, no. 1–2, pp. 11–13, May 2001.
- [7] S. B. Zhang, S.-H. Wei, A. Zunger, and H. Katayama-Yoshida, “Defect physics of the CuInSe₂ chalcopyrite semiconductor,” *Phys. Rev. B*, vol. 57, no. 16, pp. 9642–9656, Apr. 1998.
- [8] S. Lany, Y.-J. Zhao, C. Persson, and A. Zunger, “Halogen n-type doping of chalcopyrite semiconductors,” *Appl. Phys. Lett.*, vol. 86, no. 4, pp. 042109-042109-3, Jan. 2005.
- [9] C. Persson, Y.-J. Zhao, S. Lany, and A. Zunger, “n-type doping of CuInSe₂ and CuGaSe₂,” *Phys. Rev. B*, vol. 72, no. 3, p. 035211, Jul. 2005.
- [10] S. Lany and A. Zunger, “Light- and bias-induced metastabilities in Cu(In,Ga)Se₂ based solar cells caused by the (VSe-VCu) vacancy complex,” *J. Appl. Phys.*, vol. 100, no. 11, p. 113725, Dec. 2006.
- [11] S. Lany and A. Zunger, “Intrinsic DX Centers in Ternary Chalcopyrite Semiconductors,” *Phys. Rev. Lett.*, vol. 100, no. 1, p. 016401, Jan. 2008.
- [12] T. Minemoto *et al.*, “Theoretical analysis of the effect of conduction band offset of window/CIS layers on performance of CIS solar cells using device simulation,” *Sol. Energy Mater. Sol. Cells*, vol. 67, no. 1–4, pp. 83–88, Mar. 2001.
- [13] “ASTM G173-03(2012), Standard Tables for Reference Solar Spectral Irradiances: Direct Normal and Hemispherical on 37° Tilted Surface.” ASTM International, West Conshohocken, PA, 2012.
- [14] A. O. Pudov, A. Kanevce, H. A. Al-Thani, J. R. Sites, and F. S. Hasoon, “Secondary barriers in CdS–CuIn_{1-x}Ga_xSe₂ solar cells,” *J. Appl. Phys.*, vol. 97, no. 6, p. 064901, Mar. 2005.
- [15] D. Hariskos, S. Spiering, and M. Powalla, “Buffer layers in Cu(In,Ga)Se₂ solar cells and modules,” *Thin Solid Films*, vol. 480–481, pp. 99–109, Jun. 2005.

- [16] N. Naghavi *et al.*, “Buffer layers and transparent conducting oxides for chalcopyrite $\text{Cu}(\text{In,Ga})(\text{S,Se})_2$ based thin film photovoltaics: present status and current developments,” *Prog. Photovolt. Res. Appl.*, vol. 18, no. 6, pp. 411–433, Sep. 2010.
- [17] T. Wada, N. Kohara, S. Nishiwaki, and T. Negami, “Characterization of the $\text{Cu}(\text{In,Ga})\text{Se}_2/\text{Mo}$ interface in CIGS solar cells,” *Thin Solid Films*, vol. 387, no. 1–2, pp. 118–122, May 2001.
- [18] S. S. Hegedus and W. N. Shafarman, “Thin-film solar cells: device measurements and analysis,” *Prog. Photovolt. Res. Appl.*, vol. 12, no. 2–3, pp. 155–176, Mar. 2004.
- [19] R. Scheer, “Activation energy of heterojunction diode currents in the limit of interface recombination,” *J. Appl. Phys.*, vol. 105, no. 10, p. 104505, May 2009.
- [20] R. Scheer, “Towards an electronic model for $\text{CuIn}_{1-x}\text{Ga}_x\text{Se}_2$ solar cells,” *Thin Solid Films*, vol. 519, no. 21, pp. 7472–7475, Aug. 2011.
- [21] M. Pawłowski, P. Zabierowski, R. Bacewicz, H. Marko, and N. Barreau, “Photoluminescence as a tool for investigations of the junction region in $\text{Cu}(\text{In,Ga})\text{Se}_2$ -based solar cells,” *Thin Solid Films*, vol. 519, no. 21, pp. 7328–7331, Aug. 2011.
- [22] M. Pawłowski, P. Zabierowski, R. Bacewicz, N. Barreau, and A. Hultqvist, “Fill factor metastabilities in CIGSe-based solar cells investigated by means of photoluminescence techniques,” in *2011 37th IEEE Photovoltaic Specialists Conference (PVSC)*, 2011, pp. 002787–002791.
- [23] M. Igalson, M. Bodegård, and L. Stolt, “Reversible changes of the fill factor in the $\text{ZnO}/\text{CdS}/\text{Cu}(\text{In,Ga})\text{Se}_2$ solar cells,” *Sol. Energy Mater. Sol. Cells*, vol. 80, no. 2, pp. 195–207, Oct. 2003.
- [24] P.-O. Westin, U. Zimmermann, L. Stolt, and M. Edoff, “Reverse bias damage in CIGS modules,” presented at the 24th European Photovoltaic Solar Energy Conference, 21–25 September 2009, Hamburg, Germany, 2009, pp. 2967–2970.
- [25] J. Hedstrom *et al.*, “ $\text{ZnO}/\text{CdS}/\text{Cu}(\text{In,Ga})\text{Se}_2$ thin film solar cells with improved performance,” in *Conference Record of the Twenty Third IEEE Photovoltaic Specialists Conference - 1993 (Cat. No.93CH3283-9)*, 1993, pp. 364–371.
- [26] S.-H. Wei, S. B. Zhang, and A. Zunger, “Effects of Na on the electrical and structural properties of CuInSe_2 ,” *J. Appl. Phys.*, vol. 85, no. 10, pp. 7214–7218, May 1999.
- [27] M. Bodegård, K. Granath, and L. Stolt, “Growth of $\text{Cu}(\text{In,Ga})\text{Se}_2$ thin films by coevaporation using alkaline precursors,” *Thin Solid Films*, vol. 361–362, pp. 9–16, Feb. 2000.
- [28] S. Ishizuka *et al.*, “Na-induced variations in the structural, optical, and electrical properties of $\text{Cu}(\text{In,Ga})\text{Se}_2$ thin films,” *J. Appl. Phys.*, vol. 106, pp. 034908–034908, Aug. 2009.
- [29] E. Cadel, N. Barreau, J. Kessler, and P. Pareige, “Atom probe study of sodium distribution in polycrystalline $\text{Cu}(\text{In,Ga})\text{Se}_2$ thin film,” *Acta Mater.*, vol. 58, no. 7, pp. 2634–2637, Apr. 2010.
- [30] V. Fjällström *et al.*, “Potential-Induced Degradation of CuInSe Thin Film Solar Cells,” *IEEE J. Photovolt.*, vol. 3, no. 3, pp. 1090–1094, Jul. 2013.
- [31] V. Fjällström *et al.*, “Recovery After Potential-Induced Degradation of $\text{CuIn}_{1-x}\text{Ga}_x\text{Se}_2$ Solar Cells With CdS and $\text{Zn}(\text{O,S})$ Buffer Layers,” *Ieee J. Photovolt.*, vol. 5, no. 2, pp. 664–669, Mar. 2015.

- [32] T. Wada, N. Kohara, T. Negami, and M. Nishitani, "Chemical and Structural Characterization of Cu(In,Ga)Se₂/Mo Interface in Cu(In,Ga)Se₂ Solar Cells," *Jpn. J. Appl. Phys.*, vol. 35, no. 10A, p. L1253, Oct. 1996.
- [33] S. Nishiwaki, N. Kohara, T. Negami, and T. Wada, "MoSe₂ layer formation at Cu(In,Ga)Se₂/Mo Interfaces in High Efficiency Cu(In_{1-x}Ga_x)Se₂ Solar Cells," *Jpn. J. Appl. Phys.*, vol. 37, no. 1A, p. L71, Jan. 1998.
- [34] D. Abou-Ras *et al.*, "Formation and characterisation of MoSe₂ for Cu(In,Ga)Se₂ based solar cells," *Thin Solid Films*, vol. 480–481, pp. 433–438, Jun. 2005.
- [35] N. Kohara, S. Nishiwaki, Y. Hashimoto, T. Negami, and T. Wada, "Electrical properties of the Cu(In,Ga)Se₂/MoSe₂/Mo structure," *Sol. Energy Mater. Sol. Cells*, vol. 67, no. 1–4, pp. 209–215, Mar. 2001.
- [36] J. Lindahl *et al.*, "Inline Cu(In,Ga)Se₂ Co-evaporation for High-Efficiency Solar Cells and Modules," *IEEE J. Photovolt.*, vol. 3, no. 3, pp. 1100–1105, Jul. 2013.
- [37] C. Persson and A. Zunger, "Anomalous Grain Boundary Physics in Polycrystalline CuInSe₂: The Existence of a Hole Barrier," *Phys. Rev. Lett.*, vol. 91, no. 26, p. 266401, Dec. 2003.
- [38] C. Persson and A. Zunger, "Compositionally induced valence-band offset at the grain boundary of polycrystalline chalcopyrites creates a hole barrier," *Appl. Phys. Lett.*, vol. 87, no. 21, p. 211904, Nov. 2005.
- [39] Y. Yan, C.-S. Jiang, R. Noufi, S.-H. Wei, H. R. Moutinho, and M. M. Al-Jassim, "Electrically Benign Behavior of Grain Boundaries in Polycrystalline CuInSe₂ Films," *Phys. Rev. Lett.*, vol. 99, no. 23, p. 235504, Dec. 2007.
- [40] S. Siebentritt, M. Igalson, C. Persson, and S. Lany, "The electronic structure of chalcopyrites—bands, point defects and grain boundaries," *Prog. Photovolt. Res. Appl.*, vol. 18, no. 6, pp. 390–410, Sep. 2010.
- [41] M. Lammer, U. Klemm, and M. Powalla, "Sodium co-evaporation for low temperature Cu(In,Ga)Se₂ deposition," *Thin Solid Films*, vol. 387, no. 1–2, pp. 33–36, May 2001.
- [42] M. Lammer, R. Kniese, and M. Powalla, "In-line deposited Cu(In,Ga)Se₂ solar cells: influence of deposition temperature and Na co-evaporation on carrier collection," *Thin Solid Films*, vol. 451–452, pp. 175–178, Mar. 2004.
- [43] D. Rudmann *et al.*, "Sodium incorporation strategies for CIGS growth at different temperatures," *Thin Solid Films*, vol. 480–481, pp. 55–60, Jun. 2005.
- [44] P. Jackson, D. Hariskos, R. Wuerz, W. Wischmann, and M. Powalla, "Compositional investigation of potassium doped Cu(In,Ga)Se₂ solar cells with efficiencies up to 20.8%," *Phys. Status Solidi RRL – Rapid Res. Lett.*, vol. 8, no. 3, pp. 219–222, Mar. 2014.
- [45] M. A. Contreras *et al.*, "High efficiency Cu(In,Ga)Se₂-based solar cells: processing of novel absorber structures," in *Proceedings of 1994 IEEE 1st World Conference on Photovoltaic Energy Conversion - WCPEC (A Joint Conference of PVSC, PVSEC and PSEC)*, 1994, vol. 1, pp. 68–75 vol.1.
- [46] M. A. Contreras *et al.*, "High efficiency graded bandgap thin-film polycrystalline Cu(In,Ga)Se₂-based solar cells," *Sol. Energy Mater. Sol. Cells*, vol. 41–42, pp. 231–246, Jun. 1996.
- [47] I. Repins *et al.*, "19.9%-efficient ZnO/CdS/CuInGaSe₂ solar cell with 81.2% fill factor," *Prog. Photovolt. Res. Appl.*, vol. 16, no. 3, pp. 235–239, May 2008.
- [48] M. Gloeckler and J. R. Sites, "Band-gap grading in Cu(In,Ga)Se₂ solar cells," *J. Phys. Chem. Solids*, vol. 66, no. 11, pp. 1891–1894, Nov. 2005.

- [49] M. Powalla *et al.*, “High-efficiency Cu(In,Ga)Se₂ cells and modules,” *Sol. Energy Mater. Sol. Cells*, vol. 119, pp. 51–58, Dec. 2013.
- [50] C. Frisk *et al.*, “Optimizing Ga-profiles for highly efficient Cu(In, Ga)Se-2 thin film solar cells in simple and complex defect models,” *J. Phys. -Appl. Phys.*, vol. 47, no. 48, p. UNSP 485104, Dec. 2014.
- [51] R. Kamada *et al.*, “New world record Cu(In, Ga)(Se, S)₂ thin film solar cell efficiency beyond 22%,” in *2016 IEEE 43rd Photovoltaic Specialists Conference (PVSC)*, 2016, pp. 1287–1291.
- [52] T. M. Friedlmeier, D. Braunger, D. Hariskos, M. Kaiser, H. N. Wanka, and H. W. Schock, “Nucleation and growth of the CdS buffer layer on Cu(In,Ga)Se₂ thin films,” in *Conference Record of the Twenty Fifth IEEE Photovoltaic Specialists Conference - 1996*, 1996, pp. 845–848.
- [53] J. Kessler *et al.*, “Chemical bath deposition of CdS on CuInSe₂, etching effects and growth kinetics,” *Sixth Int PVSEC*, pp. 1005–1010, 1992.
- [54] T. Nakada and A. Kunioka, “Direct evidence of Cd diffusion into Cu(In,Ga)Se₂ thin films during chemical-bath deposition process of CdS films,” *Appl. Phys. Lett.*, vol. 74, no. 17, pp. 2444–2446, Apr. 1999.
- [55] T. Nakada, “Nano-structural investigations on Cd-doping into Cu(In,Ga)Se₂ thin films by chemical bath deposition process,” *Thin Solid Films*, vol. 361–362, pp. 346–352, Feb. 2000.
- [56] D. Liao and A. Rockett, “Cd doping at the CuInSe₂/CdS heterojunction,” *J. Appl. Phys.*, vol. 93, no. 11, pp. 9380–9382, May 2003.
- [57] E. B. Yousfi, T. Asikainen, V. Pietu, P. Cowache, M. Powalla, and D. Lincot, “Cadmium-free buffer layers deposited by atomic layer epitaxy for copper indium diselenide solar cells,” *Thin Solid Films*, vol. 361–362, pp. 183–186, Feb. 2000.
- [58] C. Platzer-Bjorkman, J. Kessler, and L. Stolt, “Atomic layer deposition of Zn(O,S) buffer layers for high efficiency Cu(In,Ga)Se/sub 2/ solar cells,” in *Proceedings of 3rd World Conference on Photovoltaic Energy Conversion*, 2003, 2003, vol. 1, p. 461–464 Vol.1.
- [59] A. Hultqvist, C. Platzer-Björkman, U. Zimmermann, M. Edoff, and T. Törndahl, “Growth kinetics, properties, performance, and stability of atomic layer deposition Zn–Sn–O buffer layers for Cu(In,Ga)Se₂ solar cells,” *Prog. Photovolt. Res. Appl.*, vol. 20, no. 7, pp. 883–891, Nov. 2012.
- [60] C. Platzer-Björkman, D. Abou-Ras, J. Malmström, J. Kessler, and L. Stolt, “Zn(O,S) buffer layers by atomic layer deposition in Cu(In,Ga)Se₂ based thin film solar cells: Band alignment and sulfur gradient,” *J. Appl. Phys.*, vol. 100, no. 4, p. 044506, Aug. 2006.
- [61] M. Kapilashrami *et al.*, “Soft X-ray characterization of Zn_{1-x}Sn_xO_y electronic structure for thin film photovoltaics,” *Phys. Chem. Chem. Phys.*, vol. 14, no. 29, pp. 10154–10159, Jul. 2012.
- [62] J. Lindahl, J. Keller, O. Donzel-Gargand, P. Szaniawski, M. Edoff, and T. Törndahl, “Deposition temperature induced conduction band changes in zinc tin oxide buffer layers for Cu(In,Ga)Se-2 solar cells,” *Sol. Energy Mater. Sol. Cells*, vol. 144, pp. 684–690, Jan. 2016.
- [63] J. Lindahl, J. T. Wätjen, A. Hultqvist, T. Ericson, M. Edoff, and T. Törndahl, “The effect of Zn_{1-x}Sn_xO_y buffer layer thickness in 18.0% efficient Cd-free Cu(In,Ga)Se₂ solar cells,” *Prog. Photovolt. Res. Appl.*, vol. 21, no. 8, pp. 1588–1597, Dec. 2013.
- [64] E. Fortunato, D. Ginley, H. Hosono, and D. C. Paine, “Transparent Conducting Oxides for Photovoltaics,” *MRS Bull.*, vol. 32, no. 3, pp. 242–247, Mar. 2007.

- [65] U. Rau, P. O. Grabitz, and J. H. Werner, "Resistive limitations to spatially inhomogeneous electronic losses in solar cells," *Appl. Phys. Lett.*, vol. 85, no. 24, pp. 6010–6012, Dec. 2004.
- [66] V.-T. Rangel-Kuoppa and G. Chen, "Note: Effects of several thermal glues used on temperature dependent Hall measurements," *Rev. Sci. Instrum.*, vol. 81, no. 3, p. 036102, Mar. 2010.
- [67] D. K. Schroder, *Semiconductor Material and Device Characterization*, 3rd Edition. 2005.
- [68] J. R. Sites and P. H. Mauk, "Diode quality factor determination for thin-film solar cells," *Sol. Cells*, vol. 27, Jan. 1989.
- [69] T. Ericson *et al.*, "Zn(O, S) Buffer Layers and Thickness Variations of CdS Buffer for Cu₂ZnSnS₄ Solar Cells," *Ieee J. Photovolt.*, vol. 4, no. 1, pp. 465–469, Jan. 2014.
- [70] P. M. P. Salome *et al.*, "A comparison between thin film solar cells made from co-evaporated CuIn_{1-x}Ga_xSe₂ using a one-stage process versus a three-stage process," *Prog. Photovolt.*, vol. 23, no. 4, pp. 470–478, Apr. 2015.
- [71] S. M. Sze and K. K. Ng, *Physics of Semiconductor Devices*. John Wiley & Sons, 2006.
- [72] L. C. Kimerling, "Influence of deep traps on the measurement of free-carrier distributions in semiconductors by junction capacitance techniques," *J. Appl. Phys.*, vol. 45, no. 4, pp. 1839–1845, Apr. 1974.
- [73] S. B. Zhang, S.-H. Wei, and A. Zunger, "Stabilization of Ternary Compounds via Ordered Arrays of Defect Pairs," *Phys. Rev. Lett.*, vol. 78, no. 21, pp. 4059–4062, May 1997.
- [74] L. E. Oikkonen, M. G. Ganchenkova, A. P. Seitsonen, and R. M. Nieminen, "Vacancies in CuInSe₂: new insights from hybrid-functional calculations," *J. Phys. Condens. Matter*, vol. 23, no. 42, p. 422202, 2011.
- [75] J. Pohl and K. Albe, "Intrinsic point defects in CuInSe₂ and CuGaSe₂ as seen via screened-exchange hybrid density functional theory," *Phys. Rev. B*, vol. 87, no. 24, p. 245203, Jun. 2013.
- [76] M. N. Ruberto and A. Rothwarf, "Time-dependent open-circuit voltage in CuInSe₂/CdS solar cells: Theory and experiment," *J. Appl. Phys.*, vol. 61, no. 9, pp. 4662–4669, 1987.
- [77] D. Willett and S. Kuriyagawa, "The effects of sweep rate, voltage bias and light soaking on the measurement of CIS-based solar cell characteristics," in *Conference Record of the Twenty Third IEEE Photovoltaic Specialists Conference, 1993*, 1993, pp. 495–500.
- [78] U. Rau *et al.*, "The inherent stability of Cu(In,Ga)Se₂-based solar cells," *Proc 2nd WCPEC*, 1998.
- [79] M. Igalson, P. Zabierowski, D. Przado, A. Urbaniak, M. Edoff, and W. N. Shafarman, "Understanding defect-related issues limiting efficiency of CIGS solar cells," *Sol. Energy Mater. Sol. Cells*, vol. 93, no. 8, pp. 1290–1295, Aug. 2009.
- [80] A. O. Pudov, J. R. Sites, M. A. Contreras, T. Nakada, and H.-W. Schock, "CIGS J–V distortion in the absence of blue photons," *Thin Solid Films*, vol. 480–481, pp. 273–278, Jun. 2005.
- [81] P. Zabierowski, "Electrical characterization of Cu(In,Ga)Se₂-based thin film photovoltaic devices," in *Thin Film Solar Cells: Current Status and Future Trends*, A. Bosio and A. Romeo, Eds. Nova Science Publishers, 2011.
- [82] A. Urbaniak and M. Igalson, "Relaxation of light induced metastabilities in Cu(In,Ga)Se₂ with different Ga content," *Thin Solid Films*, vol. 517, no. 7, pp. 2231–2234, Feb. 2009.

- [83] A. Urbaniak and M. Igalson, "Creation and relaxation of light- and bias-induced metastabilities in Cu(In,Ga)Se₂," *J. Appl. Phys.*, vol. 106, no. 6, p. 063720, Sep. 2009.
- [84] P. Mack, T. Ott, T. Walter, D. Hariskos, and R. Schöffler, "Optimization of reliability and metastability of CIGS solar cell parameters," in *Proc. 25th Eur. Photovoltaic Solar Energy Conf.*, 2010, pp. 3337–3340.
- [85] T. Ott, T. Walter, D. Hariskos, O. Kiowski, and R. Schöffler, "Accelerated aging and contact degradation of CIGS solar cells," in *2012 IEEE 38th Photovoltaic Specialists Conference (PVSC) PART 2*, 2012, pp. 1–7.
- [86] U. Rau, M. Schmitt, and J. Parisi, "Persistent photoconductivity in Cu(In,Ga)Se₂ heterojunctions and thin films prepared by sequential deposition," *Appl. Phys. Lett.*, vol. 73, no. 2, pp. 223–225, Jul. 1998.
- [87] T. Yanagisawa and T. Kojima, "The stability of the CuInSe₂ solar mini-module I–V characteristics under continuous and light/dark irradiation cycle tests," *Microelectron. Reliab.*, vol. 43, no. 3, pp. 503–507, Mar. 2003.
- [88] S. Chen *et al.*, "Light soaking induced doping increase and sodium redistribution in Cu(In,Ga)Se₂-based thin film solar cells," *Thin Solid Films*, vol. 582, pp. 35–38, May 2015.
- [89] P. T. Erslev, J. W. Lee, W. N. Shafarman, and J. D. Cohen, "The influence of Na on metastable defect kinetics in CIGS materials," *Thin Solid Films*, vol. 517, no. 7, pp. 2277–2281, Feb. 2009.
- [90] M. Maciaszek and P. Zabierowski, "On the magnitude of the persistent photoconductivity (PPC) effect in CIGS layers with and without sodium," in *2015 IEEE 42nd Photovoltaic Specialist Conference (PVSC)*, 2015, pp. 1–3.
- [91] P. Zabierowski and C. Platzer Björkman, "Influence of metastabilities on the efficiency of CIGSe-based solar cells with CdS, Zn(O,S) and (Zn,Mg)O buffer layers," presented at the 22nd European Photovoltaic Solar Energy Conference, Milano, 2007, 2007.
- [92] I. L. Eisgruber, J. E. Granata, J. R. Sites, J. Hou, and J. Kessler, "Blue-photon modification of nonstandard diode barrier in CuInSe₂ solar cells," *Sol. Energy Mater. Sol. Cells*, vol. 53, no. 3–4, pp. 367–377, Jun. 1998.
- [93] P. Zabierowski, U. Rau, and M. Igalson, "Classification of metastabilities in the electrical characteristics of ZnO/CdS/Cu(In,Ga)Se₂ solar cells," *Thin Solid Films*, vol. 387, no. 1–2, pp. 147–150, May 2001.
- [94] M. Maciaszek, P. Zabierowski, and K. Decock, "Modeling of the impact of Se-vacancies on the electrical properties of Cu(In,Ga)Se₂ films and junctions," *Thin Solid Films*, vol. 535, pp. 371–375, May 2013.
- [95] M. S. Hammer *et al.*, "Defect-related electronic metastabilities in chalcopyrite compounds," *Phys. B Condens. Matter*, vol. 439, pp. 60–63, Apr. 2014.
- [96] S. J. Heise, V. Gerliz, M. S. Hammer, J. Ohland, J. Keller, and I. Hammer-Riedel, "Light-induced changes in the minority carrier diffusion length of Cu(In,Ga)Se₂ absorber material," *Sol. Energy Mater. Sol. Cells*, vol. 163, pp. 270–276, Apr. 2017.
- [97] A. Krysztopa, M. Igalson, and N. Papathanasiou, "Persistent phenomena in the electrical characteristics of solar cells based on Cu(In,Ga)Se₂," *Phys. Status Solidi C*, vol. 6, no. 5, pp. 1291–1294, May 2009.
- [98] S. Lany and A. Zunger, "Limitation of the open-circuit voltage due to metastable intrinsic defects in Cu(In,Ga)Se₂ and strategies to avoid these defects," in *2008 33rd IEEE Photovoltaic Specialists Conference*, 2008, pp. 1–3.

- [99] P. Mack, T. Walter, R. Kniese, D. Hariskos, and R. Schöffler, "Reverse bias and reverse currents in CIGS thin film solar cells and modules," in *23rd European Photovoltaic Solar Energy Conference and Exhibition*, 2008, pp. 2156–2159.
- [100] S. Puttnins *et al.*, "The influence of front contact and buffer layer properties on CIGSe solar cell breakdown characteristics," in *26th European Photovoltaic Solar Energy Conference and Exhibition*, 2011.
- [101] X. Sun, J. Raguse, R. Garriss, C. Deline, T. Silverman, and M. A. Alam, "A physics-based compact model for CIGS and CdTe solar cells: From voltage-dependent carrier collection to light-enhanced reverse breakdown," in *Photovoltaic Specialist Conference (PVSC), 2015 IEEE 42nd*, 2015, pp. 1–6.
- [102] F.-C. Chiu, "A Review on Conduction Mechanisms in Dielectric Films," *Adv. Mater. Sci. Eng.*, vol. 2014, p. e578168, Feb. 2014.
- [103] D. B. Fraser and H. Melchior, "Sputter-Deposited CdS Films with High Photoconductivity through Film Thickness," *J. Appl. Phys.*, vol. 43, no. 7, pp. 3120–3127, Jul. 1972.
- [104] N. R. Pavaskar, C. A. Menezes, and A. P. B. Sinha, "Photoconductive CdS Films by a Chemical Bath Deposition Process," *J. Electrochem. Soc.*, vol. 124, no. 5, pp. 743–748, May 1977.

Acta Universitatis Upsaliensis

*Digital Comprehensive Summaries of Uppsala Dissertations
from the Faculty of Science and Technology 1501*

Editor: The Dean of the Faculty of Science and Technology

A doctoral dissertation from the Faculty of Science and Technology, Uppsala University, is usually a summary of a number of papers. A few copies of the complete dissertation are kept at major Swedish research libraries, while the summary alone is distributed internationally through the series Digital Comprehensive Summaries of Uppsala Dissertations from the Faculty of Science and Technology. (Prior to January, 2005, the series was published under the title "Comprehensive Summaries of Uppsala Dissertations from the Faculty of Science and Technology".)

Distribution: publications.uu.se
urn:nbn:se:uu:diva-319454



ACTA
UNIVERSITATIS
UPSALIENSIS
UPPSALA
2017